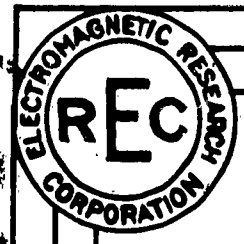

EFFECTS OF RE-ENTRY PLASMA SHEATH ON ANTENNA CHARACTERISTICS

by

M. Katzin

J. W. Marini

B. Y.-C. Koo

Final Report on

G.E. Purchase Order No. 214-361527
under
Contract AF-04-(647)-269

Prepared for

Missile & Space Vehicles Department
General Electric Co.
3198 Chestnut Street
Philadelphia, Pennsylvania

Report No. 61527-3
30 June 1960

ELECTROMAGNETIC RESEARCH CORPORATION
SHERATON BUILDING, 711-14TH ST., N.W.
WASHINGTON 5, D. C.

(5) 242025 Electromagnetic Research Corp., Bowie Md.

(6) EFFECTS OF RE-ENTRY PLASMA SHEATH ON ANTENNA CHARACTERISTICS

by

M. Katzin

J. W. Marini

B. Y.-C. Koo

(3) Final Report on

G. E. Purchase Order No. 214-361527
under
(7) Contract AF-04-(647)-269

Prepared for

Missile & Space Vehicles Department
General Electric Co.
3198 Chestnut Street
Philadelphia, Pennsylvania

ELECTROMAGNETIC RESEARCH CORPORATION
SHERATON BUILDING, 711-14TH ST., N. W.
WASHINGTON 5, D. C.

(8) Report No. 61527-3
30 June 1960

ABSTRACT

This report deals with various effects of the plasma which forms around a re-entry vehicle on antenna characteristics.

A study of numerical computations made on the IBM 704 shows that double-precision calculations are inaccurate for certain ranges of the plasma parameters, so that triple precision should be employed. A linear relation is shown to exist between the change in input admittance of a spherical slot antenna from the free-space value and the change in refractive index n_2 of the plasma, for small n_2-1, as expressed in the relation

$$\Delta Y = jK(n_2-1).$$

This suggests a convenient pre-flight calibration technique whereby in-flight measurements can be used to deduce plasma properties.

The harmonic series formulation for the input admittance is found to be impractical for values of vehicle circumference greater than about one wavelength. An alternative formulation suitable for large vehicle sizes is outlined.

A general formulation is developed for spherically inhomogeneous plasmas. It is shown that only the radial functions are affected by the inhomogeneity, so that results for the uniform plasma case can be extended to the non-uniform case by the substitution of the appropriate radial functions. It is shown, however, that the electric and magnetic modes satisfy appreciably different equations when the refractive index gradient in the plasma is large.

Investigations of the effect of the plasma on the voltage distribution along the slot did not lead to a solution of this problem. However, a procedure which appears promising is outlined.

The effect of noise generated by the plasma on the problem of signal reception

aboard a hypersonic re-entry vehicle is discussed. It is shown that the effective noise temperature of the plasma depends on the attenuation of the plasma. As a consequence, the optimum frequency for reception usually will be significantly lower than for transmission. An optimization procedure is described.

Table of Contents

EFFECTS OF RE-ENTRY PLASMA SHEATH ON ANTENNA CHARACTERISTICS

1. INTRODUCTION

This report summarizes the work done under the subcontract on the theoretical investigations into the effects which the plasma sheath generated by a high velocity vehicle re-entering the earth's atmosphere produces on the characteristics of antennas carried on the vehicle. The work reported here constitutes an extension of work carried out by the Electromagnetic Research Corporation (ERC) and reported under two previous subcontracts with the Missile and Space Vehicles Department (MSVD) [1].

In the previous work, attention was confined to uniform plasmas, and principally to strongly ionized plasmas. A strongly ionized plasma acts like a good conductor over a wide range of frequencies. Consequently, an antenna which has been matched to free space finds itself in a changed environment when the plasma forms around it. This produces a change in the input impedance of the antenna. If the antenna is used for transmission, this change in input impedance generally results in a reduction in the amount of power which is absorbed from the source. In addition, losses are introduced by the attenuation of waves transmitted through the plasma.

In a previous report [2] closed form expressions were obtained for the radiation properties of several types of antennas when surrounded by a strongly ionized plasma sheath. Particular attention was devoted to the analysis of a slotted sphere type of antenna, since this geometry is the simplest one for analysis and yet represents a fairly good approximation to the shape of practical re-entry vehicles. One of the tasks under the present subcontract was to generalize the previous work to cover:

---

* Numbers in brackets refer to References on p. 80.

(a) weaker ionization densities

(b) higher radio frequencies

(c) non-symmetric geometries.

It was anticipated that this would require a digital computation program, so that the objective was to cast the analysis in a form suitable for machine programming.

In a previous report under this subcontract [3] earlier work for the slotted sphere antenna was put in a form suitable for programming on the IBM 704 computer. Programming and calculations were carried out by MSVD for several frequencies and for a wide range of plasma ionization densities. Tabulations of the numerical results were delivered to ERC during the last month of the contract period. Examination of these results led to the recognition of several properties characteristic of the computations. One of these was a particularly simple type of relation between the change in input admittance of the antenna and the plasma characteristics for weak ionization densities. Another was that the series type of formulation used was not suitable for antennas (spheres) large relative to the wavelength, since the number of terms in the series required in order to obtain adequate convergence turned out to be too large. The results of the numerical computational program and its limitations are discussed in detail in Sec. 2 of this report.

The properties exhibited by the computed results led to additional theoretical investigations which are presented in Sec. 3. An analytical investigation of weak plasma densities led to a rather remarkable result. It was found that for a spherical geometry and a uniform plasma, the change in input admittance of the antenna when the plasma forms is proportional to the change in refractive index of the plasma sheath. The constant of pro-

portionality is in the nature of a structure constant dependent on the electrical dimensions of the vehicle. The type of result is quite general and is not limited to small vehicle sizes relative to the wavelength. From the way in which the linear proportionality was obtained, it is felt that a similar result would be obtained with other regular (separable) geometries. In addition, it is suspected that the same type of proportionality probably exists for practical vehicle geometries. This leads to a convenient and important technique for calibrating an antenna on the ground so that in-flight measurements can be used to deduce plasma properties. The details are given in Sec. 3.

Sec. 3 also contains the outline of an alternative formulation of the input impedance problem which should be suitable for large vehicle sizes. Further work along the lines indicated therein should form the basis for a computational program which should bridge the gap for high frequencies for which the earlier series formulation was found to be inadequate.

In the previous analyses it was assumed that the plasma is of constant thickness and uniform density. This is a highly idealized assumption since, in fact, the plasma sheath around a re-entry vehicle has large gradients of ionization density. The extension of the analysis to take into account these gradients is carried out in Sec. 4. It is shown that it is necessary only to replace the radial functions in the input admittance by functions appropriate to the actual variation of plasma density. It is pointed out, however, that care must be exercized not to overlook terms which are usually neglected in treatments of propagation in inhomogeneous mediums, since these terms are not negligible in re-entry plasma problems.

The analysis of the input admittance of a slot type antenna involves the voltage distribution along the slot. For a slot which is electrically short,

the voltage distribution is approximately triangular in shape, both in free space and in the presence of the plasma. For frequencies high enough so that the slot is no longer electrically short, however, the assumption of a triangular voltage distribution is probably inadequate, and, in addition, the voltage distribution may change when the plasma forms. Consequently, a method either for determining the voltage distribution or for calculating the input admittance without using assumptions regarding the voltage distribution would be desirable. Sec. 5 of this report gives the results of some work carried out on this problem. A complete solution has not been obtained, but a method of attack which may prove successful is presented.

In Sec. 6 the receiving problem aboard a re-entry vehicle is considered. In particular, the effect of noise generated in the plasma upon the reception problem is discussed. It is shown that the effective noise temperature of a receiving system depends not only on the temperature of the plasma, but also on the attenuation through the plasma at the frequency in question.

A brief summary of the work encompassed by the report, together with conclusions and recommendations for further studies, is given in Sec. 7.

2. PROGRAM OF NUMERICAL COMPUTATIONS

2.1 Introduction

In a previous report [3], an earlier solution for the input admittance of a spherical slot antenna was recast in a form suitable for numerical computation. This form was programmed for the IBM 704 computer by MSVD. Computations were carried out for a wide range of plasma densities at each of three frequencies: 14, 240, and 3000 mc. Tabulations of the results were furnished to ERC for study. The results of this computation program will be discussed in this section.

In [3] it was shown that it is preferable to calculate the difference in input admittance of the antenna in the presence of the plasma (denoted by Y) from that in some reference situation. The reference situation chosen in [3] is that where the dielectric insulating layer surrounding the antenna (and over which the plasma forms) is infinitely thick (for which the input admittance is denoted by Y_I). This choice of reference was made because the expressions in the input admittance simplify considerably. The incremental admittance then becomes

$$Y - Y_I = \frac{n_1}{120} \sum_{m=1}^{\infty} \sum_{n=0}^{n} \left(\frac{V_m}{V(0)}\right)^2 \frac{1}{\epsilon_m n(n+1)} \left[m^2 P_n^m(0)^2 F_n I_H^2 + P_n^{m\prime}(0)^2 G_n I_E^2 \right] \tag{2.1}$$

The properties of the plasma enter only into the quantities F_n and G_n, which depend on the electrical dimensions of the antenna. In these quantities the properties of the plasma enter through its complex refractive index n_2, where

$$n_2^2 = 1 - \left(\frac{x^2}{1+z^2}\right) - i\left(z\frac{x^2}{1+z^2}\right), \tag{2.2}$$

in which

$$x^2 = 81 N_e / f^2, \tag{2.3}$$

$$z = \nu / 2\pi f, \tag{2.4}$$

f being the frequency, and N_e and ν the ionization density and collision

frequency, respectively, in the plasma. Values of $Y - Y_I$ then can be computed for various plasma characteristics by programming the computations for a set of values of n_z. If one of these values is $n_z = 1$, then for this value the quantity obtained is $Y_F - Y_I$, where Y_F is the input admittance in free space. Consequently the change in input admittance upon formation of the plasma is obtained by subtracting this value from each of the other end values $Y - Y_I$:

$$\Delta Y = Y - Y_F = (Y - Y_I) - (Y_F - Y_I). \qquad (2.5)$$

This procedure was adopted since it appeared to reduce the complexity of the machine program.

In (2.1) the summation over n is shown as extending to infinity. In [3], computation only up to $n = 30$ was recommended, since pilot desk calculator computations indicated that this was sufficient to obtain convergence for the high-frequency situations of interest in the earlier studies. A procedure was indicated, however, whereby the computation of F_n and G_n, the quantities which ultimately control the convergence of the series, can be extended to larger values of n.

In this section, the numerical results obtained on the IBM 704 by MSVD will be discussed, and four characteristics of these results will be pointed out and discussed.

2.2 IBM 704 Calculations

2.2.1 Outline of Investigations

In [3], a recommended procedure was given for the calculation of input admittance in accordance with (2.1). To check the programming,* initial

---

* The programming was done by Mrs. Ruth Lyon of MSVD.

computations were made of the spherical Bessel functions occurring in F_n and G_n. These computations involve the use of recursion formulas to generate the functions of various orders. Both ascending and descending recursions are used, depending on the argument. For intermediate arguments, a check can be made by using both procedures. It was found that huge discrepancies resulted when ordinary single-precision arithmetic was used. Pilot desk computations by ERC showed that the recursion method was very sensitive to round-off error. Since the 704 carries only eight significant figures, the amount of round-off error incurred in these computations using single-precision arithmetic introduced prohibitively large errors. Accordingly, a double-precision routine was recommended as being necessary, with the possibility that triple precision might be required.

After the program was revised for double-precision computations, check values of the spherical functions agreed to four or five significant figures. Consequently, all subsequent computations were double precision. Evidence will be shown below, however, that for certain regions of plasma properties (i.e., n_e) the resulting accuracy deteriorates, so that triple precision probably is needed in these regions.

The frequencies, vehicle size, and other parameters for which calculations were carried out were specified by Dr. W. C. King of MSVD. Frequencies of 14, 240, and 3000 mc were specified. Values of x^2 and z were selected in a grid to cover an extremely wide range. Subsequently a number of intermediate points were calculated, especially for 14 mc, for which the most complete coverage was made.

As stated in Sec. 2.1, calculations were made of incremental admittance in accordance with (2.1), where Y_∞ represents the admittance when the slotted sphere is covered with a dielectric layer of infinite thickness. Plots of $Y-Y_\infty$

did not prove to be especially revealing, since, for example, the imaginary component reversed sign for certain values of η_2. When the incremental admittance ΔY as determined by (2.5) was plotted, however, certain revealing characteristics were found. In particular, the following four features became evident:

(a) A linear proportionality between ΔY and x^2, for constant z and sufficiently small x^2;

(b) an interference phenomenon at a value of x^2 near 2;

(c) a degradation of accuracy in the imaginary part of ΔY for large values of x^2 and z;

(d) apparently erroneous values of ΔY at certain "pathological" combinations of x^2 and z.

These properties and their significance will be pointed out in the discussion of some plots of ΔY to follow.

2.2.2 Dependence of ΔY on Plasma Properties

Fig. 2-1 is a plot of the real part of ΔY vs. x^2 for several values of z for a frequency of 14 mc. It can be seen that a linear proportionality exists between x^2 and both the real and imaginary parts of ΔY for x^2 below some upper value. This upper value depends on and increases with the value of z. Furthermore, a regular dependence on z also is evident.

Fig. 2-2 is the corresponding plot of the imaginary part of ΔY. For values of x^2 below about 1, the same type of linear increase with x^2 and a regular dependence on z is evident. For large x^2, however, the curves become quite irregular. In contrast, the curves of Fig. 2-1 remain very smooth and regular in this region. This feature of Fig. 2-2 will be discussed in Sec. 2.2.4.

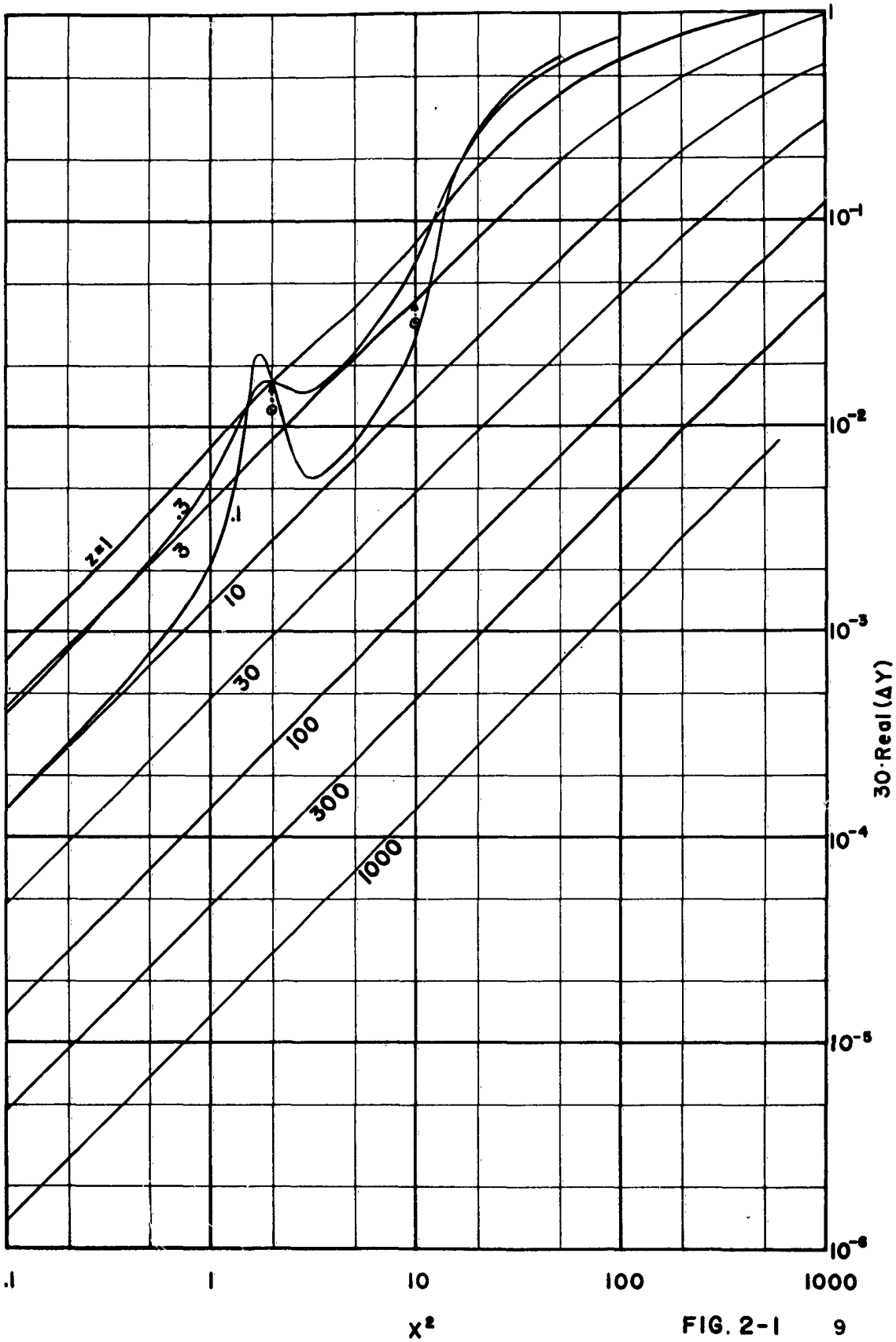
1
10^{-1}
10^{-2}
10^{-3}
10^{-4}
10^{-5}
10^{-6}
30·Real(ΔY)
z=1
.3
3
.1
10
30
100
300
1000
.1
1
10
100
1000
X^2

FIG. 2-1

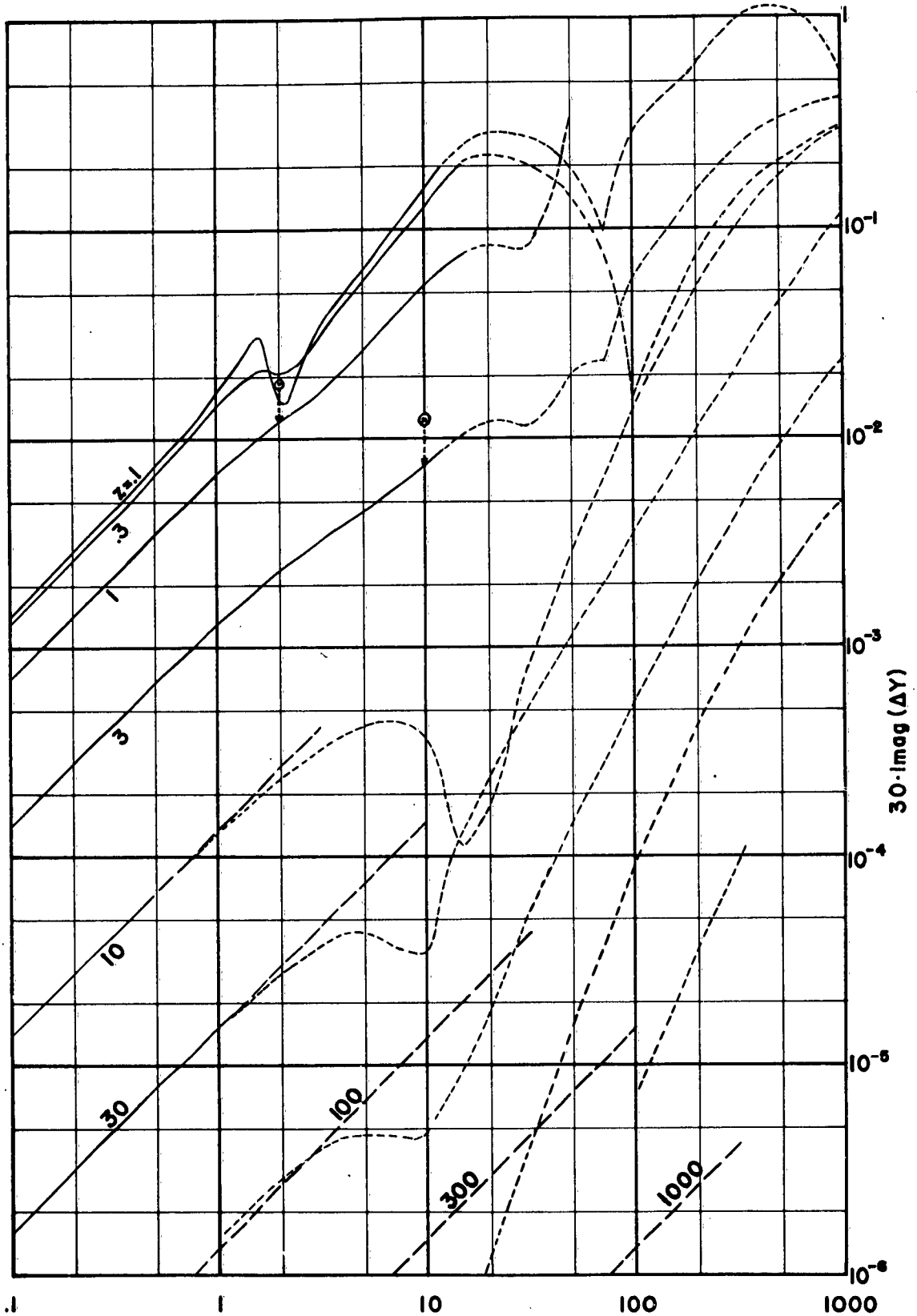
z=.1
.3
1
3
10
30
100
300
1000
1
10^{-1}
10^{-2}
10^{-3}
10^{-4}
10^{-5}
10^{-6}
30·Imag (ΔY)
.1
1
10
100
1000
X^2

FIG. 2-2

CORRECTION

Report No. 61527-3, 30 June 1960

G. E. Purchase Order 214-361527

Correction on page 11: Equation (2.7) should read

$$\mathcal{R} = \frac{Cz}{1 + z^2} \qquad (2.7)$$

Electromagnetic Research Corporation
711-14th St. N.W.
Washington, D.C.

Report No. 61527-3
30 June 1960

To show the dependence on z in the linear range more clearly, ΔY was plotted against z, for a constant value of $x^2 = 0.3$, as shown in Fig. 2-3. It was easy to see that a fit to the imaginary part of ΔY was given by a relation of the form

$$\mathcal{Q} = \frac{C}{1+z^2} \tag{2.6}$$

and the real part by

$$\mathcal{R} = \frac{C}{1+z^2} \tag{2.7}$$

where C is a constant. The solid curves in Fig. 2-3 are plots of $\mathcal{Q}$ and $\mathcal{R}$ in accordance with these relations. Since Figs. 2-1 and 2-2 show that C is proportional to x^2 for x^2 not too large, and in view of (2.2), the good agreement of the plotted points with these curves was very suggestive of the relation

$$\Delta Y = iK'(n_2^2 - 1), \tag{2.8}$$

where K' is a constant. For 14 mc, Fig. 2-3 gives $K' = 1.4 \times 10^{-2}$.

Thus we arrive at the relation (2.8) for ΔY for sufficiently small $n_2^2 - 1$. Since this region of $n_2^2 - 1$ is synonymous with $n_2 \approx 1$, (2.6) may be written as

$$\Delta Y \approx i2K'(n_2 - 1) = iK(n_2 - 1) \equiv iK\nu, \tag{2.9}$$

where $K = 2K'$, and $\nu = n_2 - 1$. It will be shown analytically in Sec. 3, in fact, that ΔY is given by (2.9) for small ν for any frequency and vehicle dimensions, K being dependent on these parameters.

A noteworthy departure from (2.8) was found for the values of ΔY corresponding to $z = 0$ in Fig. 2-1. This is classed as a "pathological" condition, which will be discussed further in Sec. 2.2.5.

2.2.3 Interference Phenomenon

In Figs. 2-1 and 2-2 a sharp increase in ΔY takes place near $x^2 = 2$ for small values of z. This produces a hump in the curve, which is more pronounced the smaller the value of z. This region is plotted in greater detail

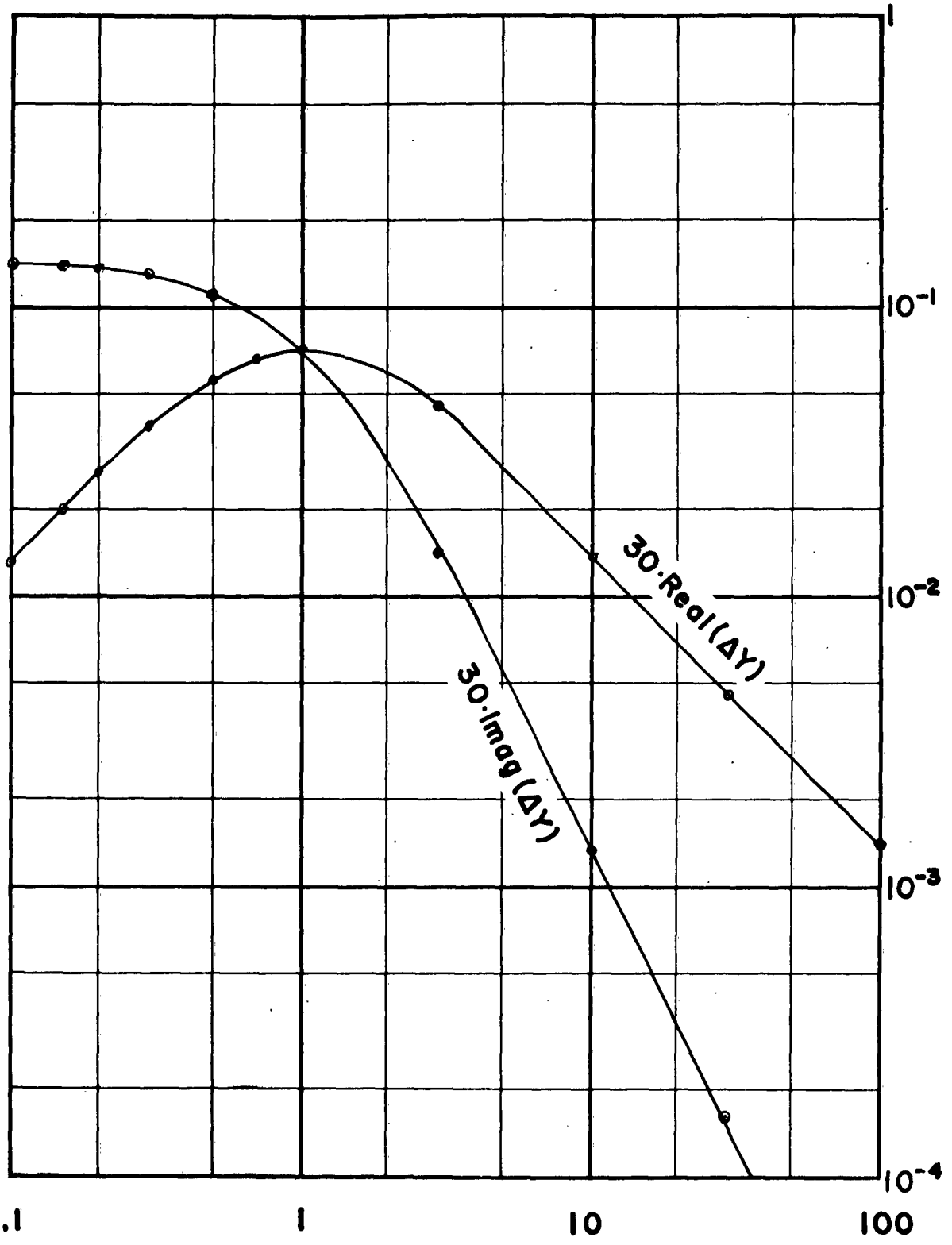

FIG. 2-3

in Figs. 2-4 and 2-5. The peak of the hump takes place at a value of χ^2 which is somewhat dependent on the value of z.

This phenomenon is suggestive of interference between the waves reflected from the inner and outer boundaries of the plasma sheath. Although for $\chi^2 > 1$ the plasma represents a barrier or attenuating layer, its electrical thickness is small enough so that the attenuation (for vanishingly small z, for example) of a round-trip passage through the sheath is quite low. A notable exception to the general trend of the other curves is exhibited by the curve for $z = 0$. As mentioned above, this curve appears to fall in the category of "pathological" values to be discussed below in Sec. 2.2.5.

The situation is analyzed qualitatively in Sec. 3.3 by means of a plane-wave analysis.

2.2.4 Reduced Accuracy of Imaginary Part of ΔY for Large z and χ^2

Fig. 2-6 shows an extension of Fig. 2-3 to larger values of z. The solid lines are the plots of (2.6) and (2.7), while the computed values are shown by the encircled points. Clearly the points for $\mathcal{G}(\Delta Y)$ depart increasingly from the curve as z increases. It will now be shown that this should be interpreted as an error in the computed values.

For z large, (2.2) approaches

$$n_2^2 - 1 \approx 2(n_2 - 1) = 2\nu = -\frac{\chi^2}{z^2} - i\frac{\chi^2}{z}.$$

Thus for $z \gg \chi^2$, ν becomes very small, decreasing as z increases. Now, as mentioned earlier, the analysis in Sec. 3 will show that

$$\Delta Y = iK\nu + O(\nu^2).$$

Thus the computed points should approach the curves more closely as z increases. Since the opposite trend takes place, the computations become suspect.

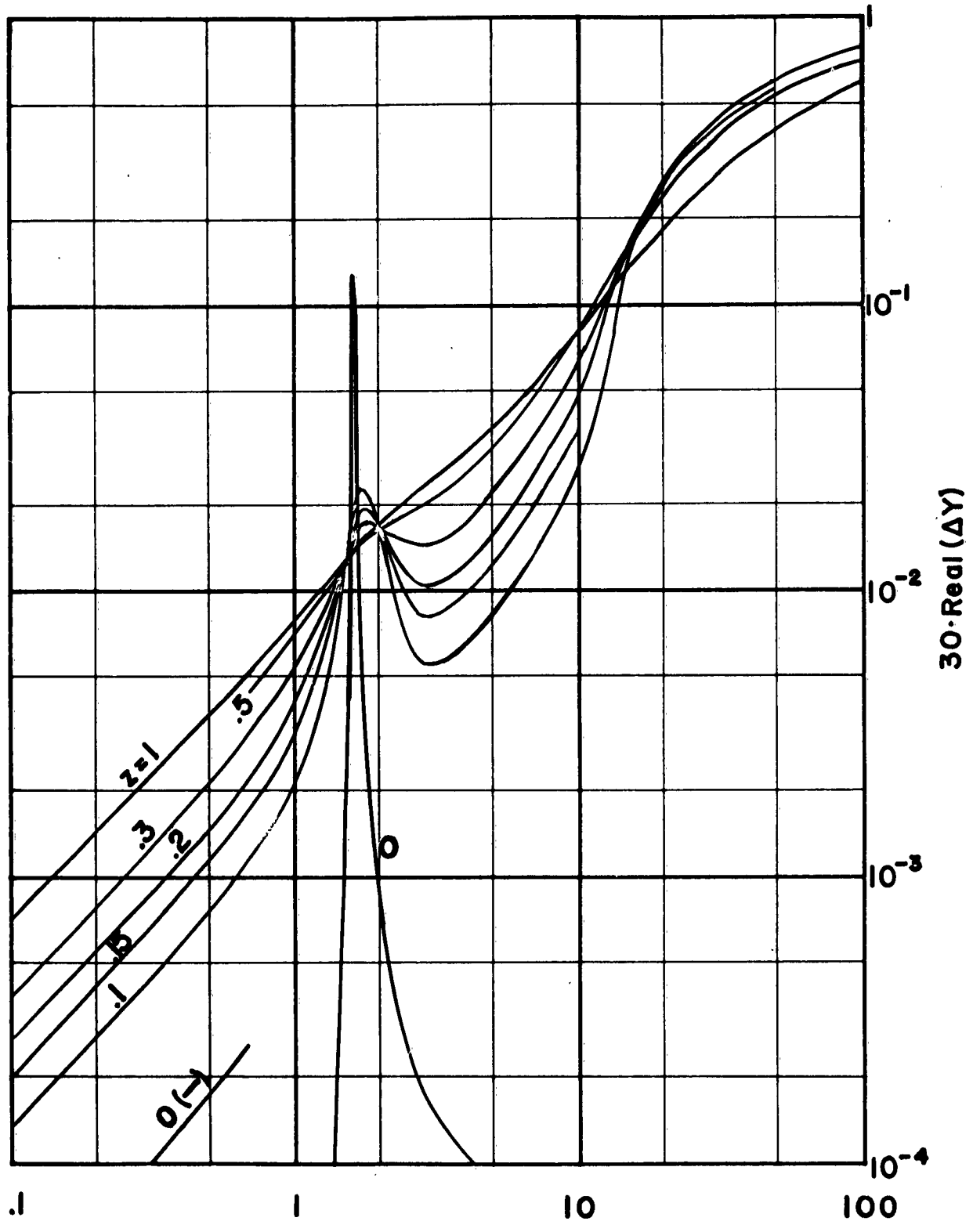

FIG. 2-4

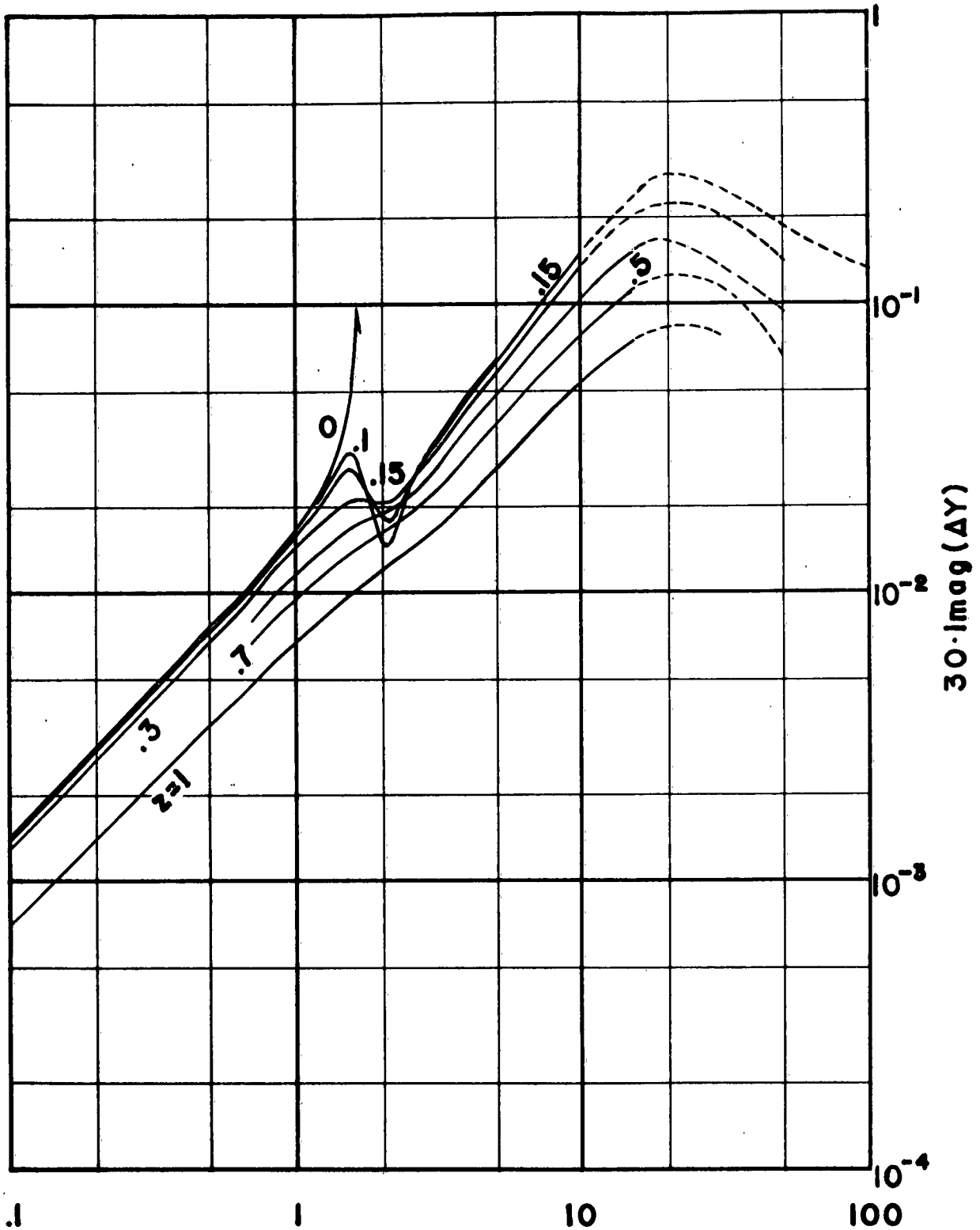

FIG. 2-5

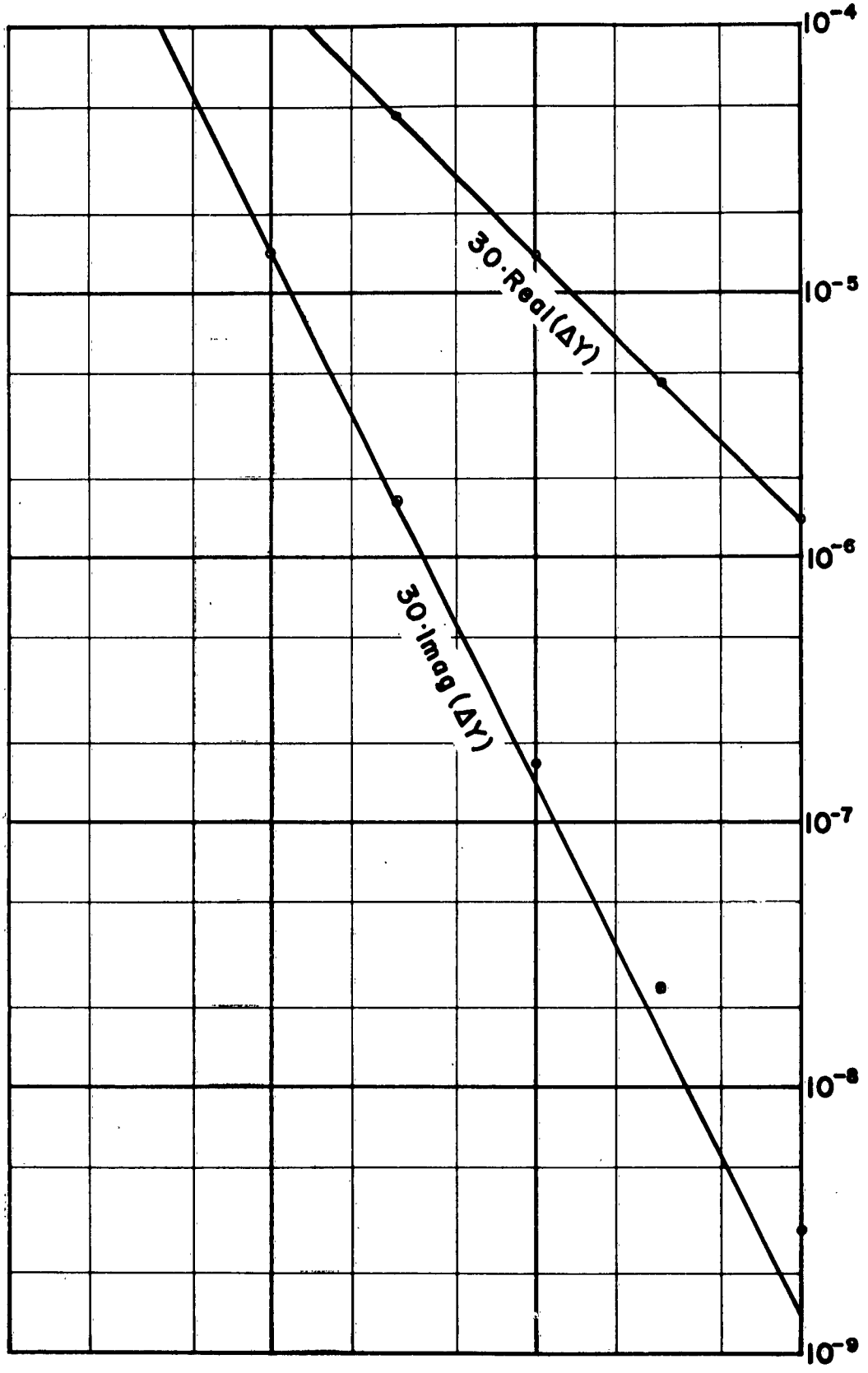

FIG. 2-6

It should be pointed out, in view of the phenomenon to be discussed in Sec. 2.2.5, that for $z \gg x^2$, the real part of $n_z^2 - 1$ becomes negligibly small relative to the imaginary part. In order words, $n_z^2 - 1$ approaches a pure imaginary quantity, while n_z^2 approaches unity.

It has been pointed out already that the curves of $\mathcal{A}(\Delta Y)$ in Fig. 2-2 become irregular for large x^2. It is believed that the curves are incorrect in these regions, and to indicate this they have been dotted. As further evidence of this inaccuracy, the values to be expected on the basis of (2.6) are shown by the dashed lines, which have been drawn up to the approximate limit of x^2 over which this relation is expected to hold ($x^2/z \approx 0.3$). As z increases, the computed values depart more and more widely from these expected values. This lends support to the conclusion that the dotted regions represent erroneous values.

The reason for this anomalous behavior of the computed values of $\mathcal{A}(\Delta Y)$ is not known. The apparent discontinuities in certain regions may be due to a change in formulation in the program which we understand was introduced for certain reasons. Why this should affect $\mathcal{A}(\Delta Y)$ and not $\mathcal{R}(\Delta Y)$ we do not know. The anomalous behavior suggests that double-precision computations on the 704 are not adequate for this problem.

2.2.5 Pathological Values

It may have been noticed already in Fig. 2-1 and 2-2 that several of the plotted points are "out of line" with respect to the smooth curve through the remaining points. Each of these points is encircled and joined by a vertical arrow to the curve on which it belongs. Curiously, every one of these "pathological" points occurs when $x^2 = 1 + z^2$.

Furthermore, it was found that when a computation was made for this combination of x^2 and z^2, a "pathological" point always developed.

It was suspected that some error had been made in the programming which resulted in this pathological behavior. However, a thorough check by Mrs. Lyon of MSVD showed that no such anomaly in the program existed. It will now be shown that round-off error is the suspected cause of these pathological values.

From (2.2), n_2^2 becomes for these values

$$n_2^2 = -iz,$$

which is pure imaginary. As noted in the preceding section, the computed values of $\mathcal{L}(\Delta Y)$ become increasingly in error as n_2^2 approaches unity for small $n_2^2 - 1$. The behavior just discussed indicates that this same type of error occurs for imaginary values of n_2^2.

Another region of anomalous behavior is the curve for $z = 0$ in Fig. 2-1. For small x^2, the values should conform to (2.8), as shown by the results of the analysis to be given in Sec. 3. However, for small x^2, the real part of the computed value of ΔY becomes negative for $z = 0$, in contradiction to the positive sign required by (2.8) and the theoretical analysis.

From the above behavior, it is suspected that the recursion calculation of the spherical Bessel functions becomes especially sensitive to round-off errors for imaginary and real values of n_2^2. Consequently it appears that, to achieve accuracy for all values of argument, a triple-precision routine would be required on the IBM 704. The anomalous behavior of $\mathcal{L}(\Delta Y)$ discussed in Sec. 2.2.4 also suggests that triple precision is necessary for this problem.

2.2.6 *K vs. f*

It was shown in Sec. 2.2.2 that, for small $\nu = n_2 - 1$ the values

of ΔY obeyed the relation

$$\Delta Y = iK\nu.$$

The dependence of the constant K on frequency will now be examined.

From plots of the computed values at the three frequencies, the values of $|K|$ in Table I were determined.

TABLE I

f, mc	$\lvert K \rvert$
14	$7.0 \cdot 10^{-3}$
240	$6.5 \cdot 10^{-3}$
3000	$7.2 \cdot 10^{-2}$

The trend exhibited by this table is for $|K|$ to increase with f. However, there is practically no change between 14 and 240 mc. In addition, there were reversals in the sign of $\mathcal{R}(\Delta Y)$ for small values of z at 240 mc, while at 3000 mc the signs were all negative.

As a result of this unexpected behavior of K, an examination was made of the values of F_n and G_n, which had been calculated as a subroutine and printed out so as to be available for study. It was found that convergence had not set in at a value of $n = 29$ for $f = 240$ and 3000 mc. It appeared, however, that a value of $n = 29$ was just about adequate for $f = 14$ mc.

From a study of the convergence properties of (2.1) as exhibited by the calculated values of F_n and G_n it is inferred that calculations would have to be carried out to about $n = 500$ for $f = 240$ mc and to about $n = 7000$ for $f = 3000$ mc. Consequently the use of (2.1) for these frequencies becomes impractical. This is the condition where the sphere is large relative to the wavelength, under which condition the harmonic series analysis becomes impractical. A method of dealing with this situation is outlined in Sec. 3.3.

2.3 Summary

From a study of the computations made by MSVD, the following four properties of the results have been recognized:

(a) a linear proportionality between the change in input admittance upon formation of the plasma, for weak plasmas, as expressed in (2.8),

(b) an interference phenomenon for small z due to the waves reflected at the inner boundary of the plasma,

(c) impaired computational accuracy for plasmas characterized by imaginary or real values of the square of the refractive index,

(d) unsatisfactory convergence properties of the series formulation (2.1) for vehicle sizes large relative to the wavelength.

In Sec. 3, theoretical investigations are made of (a), (b) and (d). The linear proportionality in (a) is demonstrated quantitatively, while a qualitative explanation of (b) is given by means of a plane-wave analysis. A procedure whereby the limitation (d) can be overcome is outlined. It appears that limitation (c) requires the use of a triple-precision program in order to obtain satisfactory accuracy with the 704 for all values of refractive index of the plasma.

3. THEORETICAL EXTENSIONS FOR A UNIFORM PLASMA

In this Section several extensions to the analytical results obtained in previous reports which were obtained under the present contract will be reported. These extensions include

(a) the analysis of weak plasmas, including a discussion of non-spherical and non-symmetrical geometries;

(b) a discussion of the interference phenomenon pointed out in Sec. 2.2.3;

(c) a formulation applicable for the condition where the sphere is large relative to the wavelength.

3.1 Weak Plasmas

In Sec. 2.2.2 it was shown that the computations indicated that, for small $\nu \equiv n_2 - 1$, ΔY obeyed the relation

$$\Delta Y = \lambda K \nu, \tag{3.1}$$

where K depends on the frequency, but not on the plasma properties. In this Section, the relation (3.1) will be derived analytically for the case of a spherical geometry. Its applicability to other geometries then will be discussed.

The method of establishing this result will be to show that for each value of the summation index n in (2.1) the corresponding term in ΔY, which will be designated by ΔY_n, contains ν as a factor.

As shown in [3], F_n and G_n are given, respectively, by

$$F_n = \frac{R_n^{M1}}{h_n^{(2)}(k_1 a)\left[h_n^{(2)}(k_1 a) - R_n^{M1} j_n(k_1 a)\right]} \tag{3.2}$$

$$G_n = \frac{R_n^{E1}}{h_n^{(2)\prime}(k_1 a)\left[h_n^{(2)\prime}(k_1 a) - R_n^{E1} j_n'(k_1 a)\right]} \tag{3.3}$$

in which R_n^{M1} is the reflection coefficient of the n^{th} magnetic mode at the boundary $r = b$, and R_n^{E1} is the corresponding reflection coefficient of the

electric mode. Expressions for R_n^{H1} and R_n^{E1} were given in [3], and will be rewritten below in a revised notation.

F_n and G_n appear in the expression for $Y - Y_I$ given in (2.1). The corresponding quantities which appear in $Y_F - Y_I$ may be denoted by $F_n^{H1^F}$ and $G_n^{H1^F}$, and the corresponding reflection coefficients by $R_n^{H1^F}$ and $R_n^{E1^F}$. It will be shown that

$$R_n^{H1} - R_n^{H1^F} = -i\nu\tau_n^H + O(\nu^2), \tag{3.4}$$

and, similarly, that

$$R_n^{E1} - R_n^{E1^F} = -i\nu\tau_n^E + O(\nu^2), \tag{3.5}$$

where τ_n^H and τ_n^E do not involve the plasma properties. These lead to the corresponding relations

$$F_n - F_n^F = i\nu f_n, \tag{3.6}$$

$$G_n - G_n^F = i\nu g_n, \tag{3.7}$$

so that

$$\Delta Y_n = i\nu K_n + O(\nu^2). \tag{3.8}$$

Consequently

$$\Delta Y = \Sigma Y_n = i\nu K + O(\nu^2), \tag{3.9}$$

which is the result to be demonstrated.

In order to make the analysis least cumbersome, it was found advantageous to introduce a simplified notation. The functions involved are the spherical Bessel, Neumann and Hankel functions, and the arguments of these functions that will be encountered are $k_1 b$, $k_2 b$, $k_3 b$, $k_2 c$, and $k_3 c$. These arguments will be denoted by the subscripts 1, 2, 3, 4, 5 respectively. Since R_n^{H1} and R_n^{E1} can be written entirely in terms of the spherical Bessel (j_n), Neumann (n_n) and Hankel ($h_n^{(2)}$) functions, the subscript n will be dropped. Consequently, for example, $j_n(k_1 b)$ is denoted by j_1, etc. Thus the following scheme is used:

$$j_n(k_1 b) \to j_1 \qquad n_n(k_1 b) \to n_1 \qquad h_n^{(2)}(k_1 b) \to h_1$$
$$j_n(k_2 b) \to j_2 \qquad n_n(k_2 b) \to n_2 \qquad h_n^{(2)}(k_2 b) \to h_2$$
$$j_n(k_3 b) \to j_3 \qquad n_n(k_3 b) \to n_3 \qquad h_n^{(2)}(k_3 b) \to h_3$$
$$j_n(k_2 c) \to j_4 \qquad n_n(k_3 c) \to n_4 \qquad h_n^{(2)}(k_2 c) \to h_4$$
$$j_n(k_3 c) \to j_5 \qquad n_n(k_3 c) \to n_5 \qquad h_n^{(2)}(k_3 c) \to h_5$$

The details will be carried through for R_n^{H1}, and then the corresponding result written down for R_n^{E1} by inspection.

From [3] we find that R_n^{H1} may be written in the determinantal form

$$R_n^{H1} = \frac{\begin{vmatrix} A & B \\ C & D \end{vmatrix}}{\begin{vmatrix} E & B \\ F & D \end{vmatrix}} = \frac{\begin{vmatrix} E - iA_2 & B \\ F - iC_2 & D \end{vmatrix}}{\begin{vmatrix} E & B \\ F & D \end{vmatrix}} = 1 - i \frac{\begin{vmatrix} A_2 & B \\ C_2 & D \end{vmatrix}}{\begin{vmatrix} E & B \\ F & D \end{vmatrix}} \equiv 1 - i\Delta^H$$

where

$$A_2 = \begin{vmatrix} n_1 & b_1 n_1' \\ j_2 & b_2 j_2' \end{vmatrix} \qquad B = \begin{vmatrix} h_3 & c_3 h_3' \\ j_4 & c_4 j_4' \end{vmatrix} \qquad E = \begin{vmatrix} j_1 & b_1 j_1' \\ j_2 & b_2 j_2' \end{vmatrix}$$
$$C_2 = \begin{vmatrix} n_1 & b_1 n_1' \\ n_2 & b_2 n_2' \end{vmatrix} \qquad D = \begin{vmatrix} h_3 & c_3 h_3' \\ n_4 & c_4 n_4' \end{vmatrix} \qquad F = \begin{vmatrix} j_1 & b_1 j_1' \\ n_2 & b_2 n_2' \end{vmatrix}$$

The corresponding expression for the free-space condition is

$$R_n^{H1^F} = 1 - i \frac{\begin{vmatrix} A_2^F & B^F \\ C_2^F & D^F \end{vmatrix}}{\begin{vmatrix} E^F & B^F \\ F^F & D^F \end{vmatrix}} \equiv 1 - i\Delta^{H^F}$$

where

$$A_2^F = \begin{vmatrix} n_1 & b_1 n_1' \\ j_3 & b_3 j_3' \end{vmatrix} \qquad B^F = \begin{vmatrix} h_3 & c_3 h_3' \\ j_3 & c_3 j_3' \end{vmatrix} = i c_3 \qquad E^F = \begin{vmatrix} j_1 & b_1 j_1' \\ j_3 & b_3 j_3' \end{vmatrix}$$
$$C_2^F = \begin{vmatrix} n_1 & b_1 n_1' \\ n_3 & b_3 n_3' \end{vmatrix} \qquad D^F = \begin{vmatrix} h_3 & c_3 h_3' \\ n_3 & c_3 n_3' \end{vmatrix} = i c_3 \qquad F^F = \begin{vmatrix} j_1 & b_1 j_1' \\ n_3 & b_3 n_3' \end{vmatrix}$$

The essential step is to develop the functions with arguments $k_2 b$ and $k_2 c$ (subscripts 2 and 4, respectively) in a Taylor's series expansion in terms of the corresponding functions of arguments $k_3 b$ and $k_3 c$ (subscripts 3 and 5, respectively). Since

$$k_2 = n_2 k_3 = k_3 + (n_2 - 1) k_3 = k_3(1+\nu),$$

we write, for example

$$j_2 \to j_n(k_2 b) = j_n\{k_3 b(1+\nu)\} = j_n(k_3 b) + \nu k_3 b\, j_n'(k_3 b) + O(\nu^2) \to j_3 + \nu b_3 j_3' + O(\nu^2),$$

$$j_2' \to \frac{d}{d(k_2 b)} j_n(k_2 b) = \frac{1}{1+\nu} \frac{d}{d(k_3 b)} \{j_3 + \nu b_3 j_3' + O(\nu^2)\} = j_3' + \nu b_3 j_3'' + O(\nu^2)$$

$$= j_3' + \nu b_3 \left[\frac{n(n+1)}{b_3^2} - 1\right] j_3 + O(\nu^2) \equiv j_3' + \nu \beta_3 j_3 + O(\nu^2),$$

where

$$\beta_3 = \frac{n(n+1)}{b_3} - b_3$$

With transformations of this type, we obtain

$$A_2 = A_2^F + \nu b_3 A_3 + O(\nu^2)$$

$$C_2 = C_2^F + \nu b_3 C_3 + O(\nu^2)$$

$$B = B^F + \nu c_3 B_3 + O(\nu^2)$$

$$D = D^F + \nu c_3 D_3 + O(\nu^2)$$

$$E = E^F + \nu b_3 E_3 + O(\nu^2)$$

$$F = F^F + \nu b_3 F_3 + O(\nu^2)$$

Then the difference between R_n^{H1} and $R_n^{H1^F}$ becomes simply

$$R_n^{H1} - R_n^{H1^F} = -i\nu \tau_n^H + O(\nu^2),$$

where

$$\tau_n^H = c_3 \left(\frac{\eta_3}{\vartheta_3} - \frac{\alpha \vartheta_3}{\varepsilon^2}\right)$$

$$\eta_3 = \begin{vmatrix} A_2^F & B_3 \\ C_2^F & D_3 \end{vmatrix} + \frac{b}{c} \begin{vmatrix} A_3 & B^F \\ C_3 & D^F \end{vmatrix}$$

$$\vartheta_3 = \begin{vmatrix} E^F & B_3 \\ F^F & D_3 \end{vmatrix} + \frac{b}{c} \begin{vmatrix} E_3 & B^F \\ F_3 & D^F \end{vmatrix}$$

$$\alpha = \begin{vmatrix} A_2^F & B^F \\ C_2^F & D^F \end{vmatrix}$$

$$\varepsilon = \begin{vmatrix} E^F & B^F \\ F^F & D^F \end{vmatrix}$$

A similar analysis may be performed for the electric modes. The result may be written down at once by inspection, since only the values of η_0, ϕ_0, a and ζ are changed:

$$R_n^{E1} - R_n^{E1^F} = -i\nu\tau_n^E + O(\nu^2).$$

Finally, there remains the incorporation of these results into the corresponding differences $F_n - F_n^F$ and $G_n - G_n^F$, which are the quantities which appear in the incremental admittance

$$\Delta Y = Y - Y_F = \sum_{n=1}^{\infty} \Delta Y_n.$$

For these we have, on denoting functions of argument $k_1 a$ by the subscript o,

$$\begin{aligned} F_n - F_n^F &= \frac{R_n^{H1}}{h_o(h_o - R_n^{H1} j_o)} - \frac{R_n^{H1^F}}{h_o(h_o - R_n^{H1^F} j_o)} \\ &= \frac{h_o(R_n^{H1} - R_n^{H1^F})}{h_o(h_o - R_n^{H1} j_o)(h_o - R_n^{H1^F} j_o)} \\ &= \frac{-i\nu\tau_n^H + O(\nu^2)}{[h_o - j_o(1 - i\Delta^H)][h_o - j_o(1 - i\Delta^{H^F})]} = \frac{-i\nu\tau_n^H + O(\nu^2)}{[-in_o + i(\Delta^{H^F} + \nu\tau_n^H)j_o][in_o + i\Delta^{H^F} j_o]} \\ &= \frac{i\nu\tau_n^H}{(n_o + ij_o\Delta^{H^F})^2} + O(\nu^2). \end{aligned}$$

Similarly,

$$G_n - G_n^F = \frac{i\nu\tau_n^E}{(n_o' + ij_o'\Delta^{E^F})^2} + O(\nu^2).$$

Since ν is a factor in $F_n - F_n^F$ and $G_n - G_n^F$ for each value of n, it is a factor in ΔY, so that we have, in general, for any electrical dimensions of the spherical antenna

$$\Delta Y = iK\nu + O(\nu^2),$$

which is (3.9), which we set out to derive. Therefore, for sufficiently small ν, ΔY is proportional to ν.

3.1.1 Non-Spherical Geometries

The result expressed in (3.9) was obtained by a Taylor's series

expansion which is valid for sufficiently weak plasmas. Consequently, since the harmonic series representation of the input admittance is absolutely convergent for any antenna size, even though it is useful for computation only for antennas which are not large relative to the wavelength, it can be used to demonstrate the validity of (3.9) for spherical antennas of any size.

For other antenna shapes for which the antenna contour is a coordinate surface in a separable coordinate system (i.e., one in which the wave equation is separable), a similar type of representation of the input admittance in a harmonic series can be carried out. It seems rather certain that in such cases a result similar to (3.9) would be obtained by the same kind of procedure as that followed above.

Re-entry vehicles generally have rotational symmetry, but seldom is the shape "separable". One is led to conjecture whether a result similar to (3.9) would apply in such cases. This would seem to be worth investigating further by means of a generalized analysis. We may express the feeling that a proportionality to ν for small ν still will be obtained.

The importance of a result of the type (3.9) for upper atmosphere probing is worth pointing out in some detail. One of the objects of analyzing the effects of a plasma sheath on antenna impedance is to be able to use in-flight impedance measurements to deduce the properties of the plasma. This has led to attempts to simulate the plasma so that pre-flight calibrations can be made of the dependence of the plasma on antenna impedance. Since a plasma reduces the dielectric constant (or real part of the refractive index) below unity, simulation of this characteristic is not a simple matter.

For weak plasmas, on the other hand, (3.9) shows that simulation in the strict sense is not necessary. The validity of (3.9), in fact, is not limited in any way

to plasma sheaths, for which ν has a negative real part, but is valid for any sheath for which ν, be it positive or negative real, or complex, is small. Hence one may use a positive real ν to obtain a calibration measurement. Now it is a simple matter to cover an antenna with a sheath of, say, polyfoam, and thus achieve a small known value of ν. By measuring the resulting change ΔY, a determination of K, or calibration, of the antenna system is achieved.

3.2 Interference Phenomenon

In Sec. 2.2.3 it was pointed out that the curves of ΔY vs. x^2 in Fig. 2-4 were suggestive of an interference phenomenon between waves reflected from the inner and outer boundaries of the plasma sheath. A qualitative analysis of this phenomenon will be developed here.

The geometry is illustrated in Fig. 3-1, where the region between a and b is occupied by the insulating layer of propagation constant k_1, and the region be-

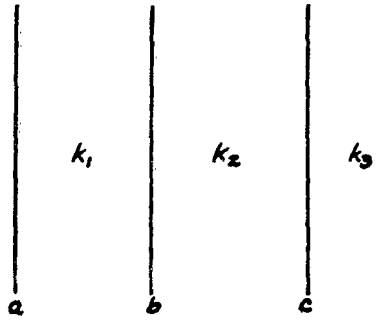

Fig. 3-1 Geometry for Analysis of Interference Phenomenon

tween b and c is the plasma of propagation constant k_2, while to the right of c is free space, represented by propagation constant k_3.

Assuming $z = 0$, we have from (2.2)

$$k_2 = n_2 k_3 = (1-x^2)^{1/2} k_3 = -i\,(x^2-1)^{1/2} k_3 . \qquad (3.10)$$

Consequently the reflection coefficient at the boundary c of waves impinging from the left is

$$\rho = \frac{k_2 - k_3}{k_2 + k_3} = \frac{1 + j(x^2-1)^{1/2}}{1 - j(x^2-1)^{1/2}} = e^{j2\theta}, \tag{3.11}$$

where

$$\theta = \tan^{-1}(x^2-1)^{1/2}. \tag{3.12}$$

At $x^2 = 2$, $\theta = 45°$, so that $2\theta = 90°$. Consequently the reflected wave then is shifted 90° in phase relative to the incident wave.

For $x^2 > 1$, k_2 is pure imaginary, as shown by (3.10). Consequently the incident wave in advancing to the right from b, as well as the reflected wave in retreating to the left from c, undergoes attenuation without phase shift. The attenuation in a one-way passage between b and c is

$$e^{-|n_2| k_3 (c-b)}.$$

At $f = 14$ mc, $c - b = 0.25$ m, and $x^2 = 2$ this amounts only to 0.64 db. Consequently the insulating layer effectively is terminated by a pure reactance for $x^2 = 2$, and this affects the input admittance markedly.

It is quite evident from (3.11) and (3.12) that the critical value of x^2, for a planar configuration, is 2, since the value of x^2 controls the phase of the reflected wave. For a non-zero value of z, the phase of the reflection coefficient is affected (as can be seen from (3.2)), and also there is an additional phase shift and an additional attenuation in the wave travel between b and c.

For a spherical geometry, there is a small departure from the relations discussed above. The curves of Figs. 2-4 and 2-5 clearly show the development of the phenomenon as a function of x^2 and z.

3.3 Large Spheres

The harmonic series representation of the input admittance as expressed in (2.1) has been shown in Sec. 2.2.6 to be impractical for computational purposes

for spheres whose circumference is a large number of wavelengths. In this Section a procedure will be outlined by means of which it appears possible to derive an alternative expression for the input admittance which is useful for large spheres. The procedure involves the following steps:

(a) Transformation of (2.1) into an integral by means of the Watson transformation;

(b) splitting up this integral into two components, one of which corresponds to the geometric optics field, the other to the diffraction field;

(c) evaluation of these integrals by appropriate methods.

The essence of the Watson transformation consists in recognizing that (2.1) is the sum of the residues of a complex integral taken over a suitable path enclosing the poles of the integrand along the positive real axis. This integral is easily seen to be

$$Y = \sum_{m=0}^{\infty} \left[\frac{V_m}{V(0)}\right]^2 \frac{1}{\epsilon_m \eta_1} \int_C \frac{e^{i\nu\pi}}{(\nu^2 - 1/4)\cos\nu\pi} \cdot \left\{ \left[\bar{P}^{m\prime}_{\nu-1/2}(0) I_E\right]^2 z_\nu^E - \left[m \bar{P}^m_{\nu-1/2}(0) I_H\right]^2 z_\nu^H \right\} d\nu, \tag{3.13}$$

where

$$\nu = n + 1/2,$$

$$z_\nu^E = Z_n^{E1}(k_1 a)/Z_n^{E1\prime}(k_1 a),$$

$$z_\nu^H = Z_n^{H1\prime}(k_1 a)/Z_n^{H1}(k_1 a).$$

The contour C is shown in Fig. 3-2.

The quantities z_ν^E and z_ν^H involve spherical functions of order n, or the ordinary cylinder functions of order $n+1/2 = \nu$.

In order to put (3.13) in a form more suitable for evaluation, we split the integral into two parts by writing

$$\frac{e^{i\nu\pi}}{\cos\nu\pi} = 1 + i\tan\nu\pi.$$

Then (3.13) splits into two parts, Y_1 and Y_2:

$$Y_1 = \sum_{m=0}^{\infty} \Lambda_m \int_C \frac{1}{\nu^2 - \frac{1}{4}} \left(\bar{I}_E^2 z_\nu^E - \bar{I}_H^2 z_\nu^H\right) d\nu, \tag{3.14}$$

$$Y_2 = i\sum_{m=0}^{\infty} \Lambda_m \int_C \frac{\tan\nu\pi}{\nu^2 - \frac{1}{4}} \left(\bar{I}_E^2 z_\nu^E - \bar{I}_H^2 z_\nu^H\right) d\nu, \tag{3.15}$$

in which

$$\Lambda_m = \frac{1}{\epsilon_m \eta_1}\left[\frac{V_m}{V(0)}\right]^2,$$

$$\bar{I}_E = \int_{\pi/2-\delta/a}^{\pi/2+\delta/a} \bar{P}_{\nu-\frac{1}{2}}^{m\prime}(\cos\theta)\sin^2\theta\, d\theta,$$

$$\bar{I}_H = \int_{\pi/2-\delta/a}^{\pi/2+\delta/a} m\,\bar{P}_{\nu-\frac{1}{2}}^{m}(\cos\theta)\, d\theta.$$

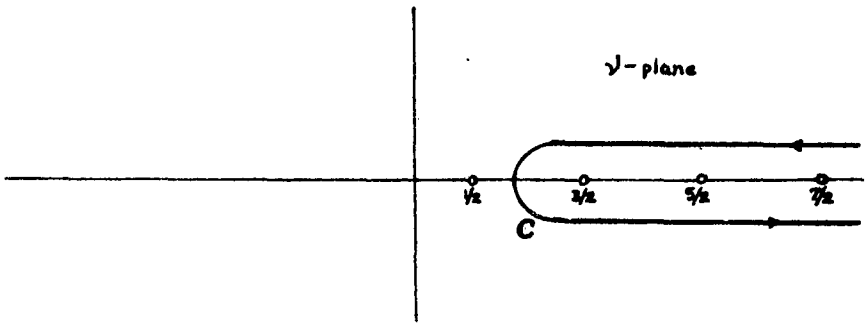

Fig. 3-2 Contour for Watson transformation

The integral in Y_1 has no poles within contour C. Consequently, asymptotic values may be inserted for the cylinder functions in z_ν^E and z_ν^H. Because of the branch point at $u = \nu$ (u denoting the argument) in the cylinder functions entering z_ν^E and z_ν^H, the appropriate asymptotic forms for these will have to be selected.

In developing the asymptotic values, the usual asymptotic expressions for the associated Legendre functions generally are used. In [4] we have shown that these functions may be replaced by a Bessel function series which is rapidly

convergent for large spheres. This representation appears to offer greater accuracy than the asymptotic expansions of the Legendre functions for spheres of intermediate size.

In the most general case, Y_1 may be expected to be decomposable into several components, corresponding to "lens" and "rainbow" terms due to corresponding action of the plasma sheath. In almost all practical cases arising in the reentry problem, however, these terms would not be expected to be of any great importance because of attenuation in the sheath.

The term Y_2 can be evaluated by residues, by deforming the contour C into loops around the poles of the integrand, which are the zeros of $Z^{H1'}_{\nu-1/2}(k,a)$ and $Z^{H1}_{\nu-1/2}(k,a)$. These residues correspond to the field which has diffracted around the sphere one or more times. Consequently, it is to be expected that Y_2 will be small compared to Y_1.

We have given only an outline of what appears to be a workable procedure for the large sphere case, since the results of the computation program became available only toward the end of the contract period. The procedure outlined follows in a general way the procedure [5] which has been found to yield satisfactory results for the computation of fields in the optical and shadow regions.

4. NON-UNIFORM PLASMAS

4.1 Introduction

In all the preceding work, the plasma has been idealized by assuming both its refractive index and thickness to be constant. Both of these assumptions are far from the true situation in re-entry plasmas. Consequently it is desirable to extend the treatment to a more realistic approximation. In this connection, knowledge of the plasma shape and properties probably is still only in a crude state. Nevertheless, a more realistic approximation than that of a homogeneous plasma should not be difficult to obtain.

In this Section, the previous treatment will be refined to take into account an inhomogeneous plasma, but with the restriction that the stratification be spherically symmetrical, so that the thickness of the plasma is constant. In this case it turns out that the previous results are modified by the replacement of the radial functions (spherical Bessel functions) by functions appropriate to the variation of refractive index with the radial distance. Beyond this, an important difference enters, in that the radial functions for the electric modes are not the same as the radial functions for the magnetic modes, since they satisfy different differential equations.

A rather general treatment of the problem of propagation in a non-homogeneous spherically-stratified medium was given by B. Friedman [6]. Friedman's analysis was aimed at propagation through the earth's atmosphere. Consequently, he was able to neglect certain terms arising from the gradient of refractive index which are small in that problem. In the re-entry plasma problem, however, these terms no longer are negligible. In addition, Friedman treated the case of point electric or magnetic dipole sources at a finite distance above the surface. Here we shall

be interested in the distributed surface source representing an excited slot.

In view of these differences, it seems desirable to formulate the analysis rather fully, in order to bring out the differences between the homogeneous and the inhomogeneous plasma. This will be carried to the point where the results parallel those for the homogeneous plasma, so that similar procedures then can be followed.

4.2 Formulation

The underlying geometry will be the same as in the homogeneous case: a slotted perfectly-conducting sphere is energized by a voltage source at its center. The sphere is covered with a uniform insulating layer of thickness $b-a$ and propagation constant k_1. Overlying this is a spherically stratified plasma of varying refractive index $n_2 = n_2(R)$, of thickness $c-b$. The plasma terminates in free space, either abruptly if c is finite, or gradually if $c \to \infty$.

As in the homogeneous case, the fields may be separated into electric and magnetic modes. The electric modes may be derived from an electric Hertz vector potential $\underset{\sim}{\Pi}^E$ in virtue of the Maxwell equation

$$\operatorname{div} \underset{\sim}{E} = 0.$$

This Hertz vector, however, does not satisfy the wave equation. But by writing

$$\underset{\sim}{\Pi}^E = k_2 \underset{\sim}{R} P^E, \tag{4.1}$$

then it may be shown that P^E satisfies the modified wave equation

$$\nabla^2 P^E + \bar{k}_2^2 P^E = 0, \tag{4.2}$$

where

$$\bar{k}_2^2 = k_2^2 - k_2 \frac{d^2(1/k_2)}{dR^2} = k_0^2 \left(n_2^2 - \frac{n_2}{k_0^2} \frac{d^2(1/n_2)}{dR^2} \right) \equiv k_0^2 \bar{n}_2^2. \tag{4.3}$$

The quantity $\bar{n}_2$ may be considered as an effective refractive index for the electric modes.

The electric and magnetic field strengths of the electric modes are derivable from the equations

$$\underset{\sim}{E}^{E} = \frac{1}{k_2^2}\, curl\, curl\, \underset{\sim}{\Pi}^{E} = \underset{\sim}{\Pi}^{E} + grad\left(\frac{1}{k_2^2}\frac{\partial \Pi^{E}}{\partial R}\right), \tag{4.4}$$

$$\underset{\sim}{H}^{E} = -\frac{1}{i\omega\mu}\, curl\, \underset{\sim}{\Pi}^{E} = -\frac{1}{i\omega\mu}\, curl\,(k_2 \underset{\sim}{R} P^{E}). \tag{4.5}$$

It should be noted that in these equations k_2 appears rather than $\bar{k}_2$.

The magnetic modes are due to source distributions which are characterized by div $\underset{\sim}{Q} = 0$. Circular current distributions have this property. The fields of magnetic modes are derivable from a radial Hertz vector potential $\underset{\sim}{\Pi}^{H}$, which, like $\underset{\sim}{\Pi}^{E}$, does not satisfy the wave equation. But by writing

$$\underset{\sim}{\Pi}^{H} = k_2^2 \underset{\sim}{R} P^{H}, \tag{4.6}$$

it turns out that P^{H} satisfies the ordinary wave equation

$$\nabla^2 P^{H} + k_2^2 P^{H} = 0. \tag{4.7}$$

The electric and magnetic field strengths of the magnetic modes are derivable from the equations

$$\underset{\sim}{E}^{H} = \frac{1}{k_2^2}\, curl\, \underset{\sim}{\Pi}^{H} = \frac{1}{k_2^2}\, curl\,(k_2^2 \underset{\sim}{R} P^{H}), \tag{4.8}$$

$$\underset{\sim}{H}^{H} = -\frac{1}{i\omega\mu}\left[\underset{\sim}{\Pi}^{H} + grad\frac{\partial}{\partial R}\left(\frac{\Pi^{H}}{k_2^2}\right)\right] = -\frac{1}{i\omega\mu}\left[k_2^2 \underset{\sim}{R} P^{H} + grad\frac{\partial}{\partial R}(R P^{H})\right]. \tag{4.9}$$

The advantage of writing the Hertz vectors $\underset{\sim}{\Pi}^{E}$, $\underset{\sim}{\Pi}^{H}$ in terms of the scalar functions P^{E}, P^{H}, respectively, is that the latter quantities are solutions of scalar wave equations whose separation properties are well known. Thus, (4.2) may be separated in spherical coordinates by writing

$$R P^{E} = T(\theta)\, U^{E}(R)\, V(\varphi), \tag{4.10a}$$

where

$$\frac{d^2 V}{d\varphi^2} + m^2 V = 0, \tag{4.10b}$$

$$\frac{1}{\sin\theta}\frac{d}{d\theta}\left(\sin\theta \frac{dT}{d\theta}\right) + \left(s^2 - \frac{m^2}{\sin^2\theta}\right) T = 0, \tag{4.10c}$$

$$\frac{d^2U^E}{dR^2} + \left(\bar{k}_2^2 - \frac{s^2}{R^2}\right)U^E = 0. \qquad (4.10d)$$

The boundary conditions demand the continuity of the θ- and φ-components of E and H at the boundaries of the plasma. These lead to the requirement that

$$k_2 U^E \quad \text{and} \quad \frac{1}{k_2^2}\frac{d(k_2 U^E)}{dR}$$

be continuous across the boundaries.

Similarly, for the magnetic modes one obtains separable solutions of (4.7) by writing

$$RP^H = T(\theta)U^H(R)V(\varphi), \qquad (4.11a)$$

where T and V are solutions of (4.10c), and (4.10b), respectively, as before, but $U^H(R)$ is a solution of

$$\frac{d^2U^H}{dR^2} + \left(k_2^2 - \frac{s^2}{R^2}\right)U^H = 0. \qquad (4.11b)$$

Thus it is clear that the magnetic radial functions U^H satisfy a somewhat different differential equation than the electric radial functions U^E. The difference resides in the appearance of the modified radial propagation constant $\bar{k}_2$ in (4.10d), while in (4.11b) k_2 appears unmodified.

For the magnetic modes, the boundary conditions require the continuity of

$$U^H \quad \text{and} \quad \frac{dU^H}{dR}$$

across the boundaries of the plasma.

If one chooses the separation constant s^2 to be

$$s^2 = n(n+1)$$

then a finite solution of (4.10c) is

$$T = \bar{P}_n^m(\cos\theta).$$

Consequently, a harmonic series representation for the fields, and ultimately of the input admittance Y, is obtained similar to that in (2.1). The essential dif-

ference lies in the radial functions for medium ②. Instead of the spherical Hankel functions which appear (2.1), the corresponding solutions of (4.10d) appear.

For the magnetic modes, the same type of harmonic series representation is permissible, the only difference being that the radial functions are the appropriate solutions of (4.11b).

Thus the fields are derivable from the radial Hertz potentials

$$\pi^E = \sum_{n=1}^{\infty} \sum_{m=0}^{n} a^E_{nm}\, k_2\, U^E_n(R)\, \bar{P}^m_n(\cos\theta) \cos m\varphi, \tag{4.12a}$$

$$\pi^H = \sum_{n=1}^{\infty} \sum_{m=0}^{n} a^H_{nm}\, k_2^2\, U^H_n(R)\, \bar{P}^m_n(\cos\theta) \sin m\varphi. \tag{4.12b}$$

The field components are obtained from (4.4) and (4.5) for the electric modes and from (4.8) and (4.9) for the magnetic modes. The tangential components are

$$\left.\begin{aligned}
E_\theta &= \frac{1}{R} \sum_n \sum_m \left\{ a^E_{nm} \frac{(k_2 U^E_n)'}{k_2^2} \bar{P}^{m\prime}_n + a^H_{nm} U^H_n \frac{m \bar{P}^m_n}{\sin\theta} \right\} \cos m\varphi, \\
E_\varphi &= -\frac{1}{R} \sum_n \sum_m \left\{ a^E_{nm} \frac{(k_2 U^E_n)'}{k_2^2} \frac{m \bar{P}^m_n}{\sin\theta} + a^H_{nm} \bar{P}^{m\prime}_n \right\} \sin m\varphi, \\
H_\theta &= \frac{1}{i\omega\mu R} \sum_n \sum_m \left\{ a^E_{nm} k_2 U^E_n \frac{m \bar{P}^m_n}{\sin\theta} - a^H_{nm} U^{H\prime} \bar{P}^{m\prime}_n \right\} \sin m\varphi, \\
H_\varphi &= \frac{1}{i\omega\mu R} \sum_n \sum_m \left\{ a^E_{nm} k_2 U^E_n \bar{P}^{m\prime}_n - a^H_{nm} U^{H\prime}_n \frac{m \bar{P}^m_n}{\sin\theta} \right\} \cos m\varphi.
\end{aligned}\right\} \tag{4.13}$$

In the above, $(k_2 U^E_n)'$ denotes $\frac{d}{dR}(k_2 U^E_n)$ and $\bar{P}^{m\prime}_n$ denotes $\frac{d}{d\theta}(\bar{P}^m_n(\cos\theta))$.

Equations (4.13) are valid for the inhomogeneous (but spherically-stratified) plasma, medium ②, as well as the homogeneous insulating layer, medium ①, and the outer free space region ③. Only the radial functions U^E_n, U^H_n will differ for each region. The forms of the functions in each region are determined by the differential equations which they satisfy and the boundary conditions.

In order to determine the fields by means of the boundary conditions, we assume the following forms for U^E_n and U^H_n:

$$U^{E1}_n = h^{(2)}_n(k_1 R) - R^E_n j_n(k_1 R), \qquad U^{H1}_n = h^{(2)}_n(k_1 R) - R^H_n j_n(k_1 R), \tag{4.14a}$$

$$U_n^{E2} = T_n^E (v_n^{(2)} - \rho_n^E v_n^{(1)}), \qquad U_n^{H2} = T_n^H (w_n^{(2)} - \rho_n^H w_n^{(1)}). \tag{4.14b}$$

$$U_n^{E3} = \tau_n^E h_n^{(2)}(k_3 R), \qquad U_n^{H3} = \tau_n^H h_n^{(2)}(k_3 R). \tag{4.14c}$$

$v_n^{(2)}$ and $v_n^{(1)}$ are, respectively, outgoing and incoming wave solutions of (4.10d) for medium ②, while $w_n^{(2)}$ and $w_n^{(1)}$ are the corresponding solutions of (4.11b). $R_n^{E,H}$ and $\rho_n^{E,H}$ are reflection coefficients at the boundaries of the sheath, and $T_n^{E,H}$ and $\tau_n^{E,H}$ are the corresponding transmission coefficients.

4.3 Determination of Amplitude Coefficients

The amplitude coefficients a_{nm}^E and a_{nm}^H are determined from the prescribed boundary values of E_θ and E_φ on the conducting sphere $R = a$:

$$\left.\begin{aligned} &E_\varphi(a,\theta,\varphi) = 0, \\ &E_\theta(a,\theta,\varphi) = \frac{1}{2s}\sum_{p=0}^{\infty}{}' V_p \cos p\varphi \left[\mathcal{H}\left(\theta - \tfrac{\pi}{2} + \tfrac{s}{a}\right) - \mathcal{H}\left(\theta - \tfrac{\pi}{2} - \tfrac{s}{a}\right)\right] \end{aligned}\right\} \tag{4.15}$$

where $\mathcal{H}(x)$ is the Heaviside step function. From the reciprocity theorem and the orthogonality properties of the trigonometric and associated Legendre functions [7], these coefficients are found to be

$$\begin{aligned} a_{nm}^E &= -\frac{\epsilon_m a}{2n(n+1)} \frac{1}{U_n^{E'}(a)} \int_{-\pi}^{\pi}\int_{0}^{\pi} E_\theta(a,\theta,\varphi)\, \bar{P}_n^{m\prime} \sin\theta \cos m\varphi \, d\theta \, d\varphi \\ &= -\frac{V_m}{n(n+1)} \frac{\bar{P}_n^{m\prime}(0)\, I_E}{k_i U_n^{E'}(a)}, \end{aligned} \tag{4.16a}$$

$$\begin{aligned} a_{nm}^H &= \frac{\epsilon_m a}{2n(n+1)} \frac{1}{U_n^{H}(a)} \int_{-\pi}^{\pi}\int_{0}^{\pi} E_\theta(a,\theta,\varphi) \frac{m\bar{P}_n^m}{\sin\theta} \cos m\varphi \, d\theta \, d\varphi \\ &= \frac{V_m}{n(n+1)} \frac{m\bar{P}_n^m(0) I_H}{U_n^H(a)}. \end{aligned} \tag{4.16b}$$

where

$$I_E = \frac{a}{2s} \int_{\frac{\pi}{2}-\frac{s}{a}}^{\frac{\pi}{2}+\frac{s}{a}} \frac{\bar{P}_n^{m\prime}(\cos\theta)}{\bar{P}_n^{m\prime}(0)} \sin\theta \, d\theta$$

and

$$I_H = \frac{a}{2s}\int_{\frac{\pi}{2}-\frac{s}{2}}^{\frac{\pi}{2}+\frac{s}{2}} \frac{\bar{P}_n^m(\cos\theta)}{\bar{P}_n^m(0)}\,d\theta$$

and

$$\epsilon_m = \begin{cases} 1, & m = 0, \\ 2, & m \neq 0. \end{cases}$$

Except for the functions $U_n^{E'}(a)$ and $U_n^{H}(a)$, (4.16a) and (4.16b) are the same as in the case of the homogeneous plasma.

By introducing the values of (4.15a) and (4.15b) into (4.13), expressions for the field components in terms of the exciting voltage applied to the slot are obtained. These then can be used to solve for the fields and the radiation and impedance properties of the antenna.

4.4 Determination of Reflection and Transmission Coefficients

Application of the boundary conditions, i.e. the continuity of

$$kU^E,\ U^H,\ \frac{(kU^E)'}{k^2} \text{ and } U^{H'}$$

at the boundaries of the sheath, leads to the following values for the reflection coefficients:

$$\rho_n^E = \frac{C_1}{D_1} \tag{4.17a}$$

$$R_n^E = \frac{\begin{vmatrix} A_1 & B_1 \\ C_1 & D_1 \end{vmatrix}}{\begin{vmatrix} E_1 & F_1 \\ C_1 & D_1 \end{vmatrix}} \tag{4.17b}$$

where

$$A_1 = \begin{vmatrix} k_1^2 h_1 & h_1' \\ [k_2^2 U_n^{(2)}]_2 & [k_2 U_n^{(2)}]_2' \end{vmatrix} \qquad B_1 = \begin{vmatrix} k_1^2 h_1 & h_1' \\ [k_2^2 U_n^{(4)}]_2 & [k_2 U_n^{(4)}]_2' \end{vmatrix}$$

$$C_1 = \begin{vmatrix} k_3^2 h_3 & h_3' \\ [k_2^2 U_n^{(2)}]_4 & [k_2 U_n^{(2)}]_4' \end{vmatrix} \qquad D_1 = \begin{vmatrix} k_3^2 h_3 & h_3' \\ [k_2^2 U_n^{(1)}]_4 & [k_2 U_n^{(1)}]_4' \end{vmatrix}$$

$$E_1 = \begin{vmatrix} k_1^2 j_1 & j_1' \\ [k_3^2 U_n^{(2)}]_2 & [k_3 U_n^{(2)}]_2' \end{vmatrix} \qquad F_1 = \begin{vmatrix} k_1^2 j_1 & j_1' \\ [k_2^2 U_n^{(1)}]_2 & [k_2 U_n^{(1)}]_2' \end{vmatrix}$$

In terms of these reflection coefficients, the transmission coefficients are

$$T_n^E = \frac{k_1(h_1 - R_n^E j_1)}{[k_2 v_n^{(2)}]_2 - \rho_n^E [k_2 v_n^{(1)}]_2}, \tag{4.18a}$$

$$\tau_n^E = \frac{[k_2 v_n^{(2)}]_4 - \rho_n^E [k_2 v_n^{(1)}]_4}{k_3 h_3} T_n^E. \tag{4.18b}$$

Similarly, for the magnetic modes

$$\rho_n^H = \frac{C_2}{D_2}, \tag{4.19a}$$

$$R_n^H = \frac{\begin{vmatrix} A_2 & B_2 \\ C_2 & D_2 \end{vmatrix}}{\begin{vmatrix} E_2 & F_2 \\ C_2 & D_2 \end{vmatrix}}, \tag{4.19b}$$

$$T_n^H = \frac{k_1(h_1 - \rho_n^H j_1)}{[w_n^{(2)}]_2 - \rho_n^H [w_n^{(1)}]_2}, \tag{4.20a}$$

$$\tau_n^H = \frac{[w_n^{(2)}]_4 - \rho_n^H [w_n^{(2)}]_4}{k_3 h_3} T_n^H, \tag{4.20b}$$

where

$$A_2 = \begin{vmatrix} h_1 & h_3 \\ [v_n^{(2)}]_2 & [v_n^{(1)}]_2' \end{vmatrix} \qquad B_2 = \begin{vmatrix} h_3 & h_3' \\ [v_n^{(1)}]_4 & [v_n^{(1)}]_4' \end{vmatrix}$$

$$C_2 = \begin{vmatrix} h_1 & h_1' \\ [v_n^{(2)}]_4 & [v_n^{(2)}]_4' \end{vmatrix} \qquad D_2 = \begin{vmatrix} h_3 & h_3' \\ [v_n^{(1)}]_4 & [v_n^{(1)}]_4' \end{vmatrix}$$

$$E_2 = \begin{vmatrix} j_1 & j_1' \\ [v_n^{(2)}]_2 & [v_n^{(2)}]_2' \end{vmatrix} \qquad F_2 = \begin{vmatrix} j_1 & j_1' \\ [v_n^{(1)}]_4 & [v_n^{(1)}]_4' \end{vmatrix}$$

4.5 Input Admittance

The input admittance may be formulated in the same way as in [2] for the case of a homogeneous plasma. The admittance is obtained from the relation

$$Y = \frac{1}{[V(0)]^2} \int_{-\pi}^{\pi} \int_{0}^{\pi} E_\theta(a,\theta,\varphi)\, H_\varphi(a,\theta,\varphi)\, a^2 \sin\theta \, d\theta \, d\varphi. \tag{4.21}$$

The result is

$$Y = \sum_n \sum_m -j \left[\frac{V_m}{V(0)}\right]^2 \frac{2\pi}{\epsilon_m \eta_1} \left\{ \tau_n^E \frac{[\bar{P}_n^{m\prime}(0) I_E]^2}{n(n+1)} - \tau_n^H \frac{[m \bar{P}_n^m(0) I_H]^2}{n(n+1)} \right\}, \tag{4.21a}$$

where

$$\tau_n^E = \frac{k_1(h_0 - R_n^E j_0)}{h_0' - R_n^E j_0'}, \tag{4.22a}$$

$$\varsigma_n^H = \frac{h_0' - R_n^H j_0'}{k_1 (h_0 - R_n^H j_0)} . \qquad (4.22b)$$

(4.21) is entirely analogous to (2.1), the only difference being in the replacement of the radial functions $\mathcal{Z}_n^E$, $\mathcal{Z}_n^H$ (defined by

$$\mathcal{Z}_n^E = Z_n^{E1}(k_1 a) / Z_n^{E1'}(k_1 a), \qquad (4.23a)$$

$$\mathcal{Z}_n^H = Z_n^{H1'}(k_1 a) / Z_n^{H1}(k_1 a) . \qquad (4.23b)$$

as in Sec. 3.3) by the functions ς_n^E and ς_n^H, respectively.

4.6 Radiation Field

The radiation field is obtained by replacing the radial functions U_n^{E3} and U_n^{H3} by their asymptotic values. Since these radial functions are the same as in the homogeneous case, except for the values of the transmission coefficients, the form of the radiation pattern is essentially the same in both cases. Some important differences can arise, however, from the variation of the transmission coefficients with direction. In some cases, cut-off can set in at certain angles due to substantially total internal reflection at the plasma sheath. This phenomenon can be affected appreciably by the nature of the refractive index gradient. This phenomenon also can take place to a different degree for the electric and magnetic modes, due to the fact that the corresponding radial functions for these modes satisfy different differential equations. The difference lies in the appearance of the effective refractive index $\overline{n}_2$ in the radial equation for the electric modes, while the equation for the magnetic modes contains the refractive index n_2. This difference will be discussed in greater detail below.

4.7 Effective Refractive Index for Electric and Magnetic Modes

To illustrate the significance of the difference between $\overline{n}_2$ and n_2,

consider the case of a plasma which has a refractive index which is zero at its inner radius $R = b$, which grows to a maximum at a radius R_m and then decays (say exponentially) to zero. This can be represented, say, by

$$n_2^2 = A(R-b)\,e^{-B(R-b)}.$$

The maximum value of n_2 occurs where

$$R_m - b = 1/B.$$

Hence

$$n_2^2 = A(R-b)\,e^{-(R-b)/(R_m-b)},$$

or, on putting

$$R - b = r,$$

$$n_2^2 = A\,r\,e^{-r/r_m}. \tag{4.24}$$

This variation is illustrated in Fig. 4-1 by the solid curve.

To find $\bar{n}_2^2$, we have

$$n_2 \frac{d^2(1/n_2)}{dR^2} = \frac{e^{-r/2r_m}}{r^{1/2}} \frac{d^2}{dr^2}\left(\frac{e^{r/2r_m}}{r^{1/2}}\right) = \frac{1}{4}\left[\left(\frac{1}{r} - \frac{1}{r_m}\right)^2 + \frac{2}{r^2}\right].$$

Hence

$$\begin{aligned}\bar{n}_2^2 &= n_2^2 - \frac{n_2}{k_3^2}\frac{d^2}{dr^2}(1/n_2) \\ &= A\,r\,e^{-r/r_m} - \frac{1}{4}\left[\left(\frac{1}{k_3 r} - \frac{1}{k_3 r_m}\right)^2 + \frac{2}{(k_3 r)^2}\right].\end{aligned}$$

Since the bracketed quantity is always positive, $\bar{n}_2^2$ is always less than n_2^2. This is shown by the dotted curve in Fig. 4-1. Whereas n_2^2 is everywhere finite, $\bar{n}_2^2$ is $-\infty$ at $r = 0$. Thus $\bar{k}_2^2 = k_0^2 \bar{n}_2^2$ in (4.10d) has a singularity at $r = 0$, whereas $k_2^2 = n_2^2 k_0^2$ in (4.11b) is regular at $r = 0$.

As in the above example, the magnitude of the difference between $\bar{n}_2^2$ and n_2^2 depends on the "curvature" of the reciprocal refractive index measured in terms of the free-space wavelength. Thus at sufficiently high frequencies (small k_3) this difference becomes small except very near $r = 0$ (the inner boundary of the plasma), where the model given by (4.24) has discontinuous derivatives.

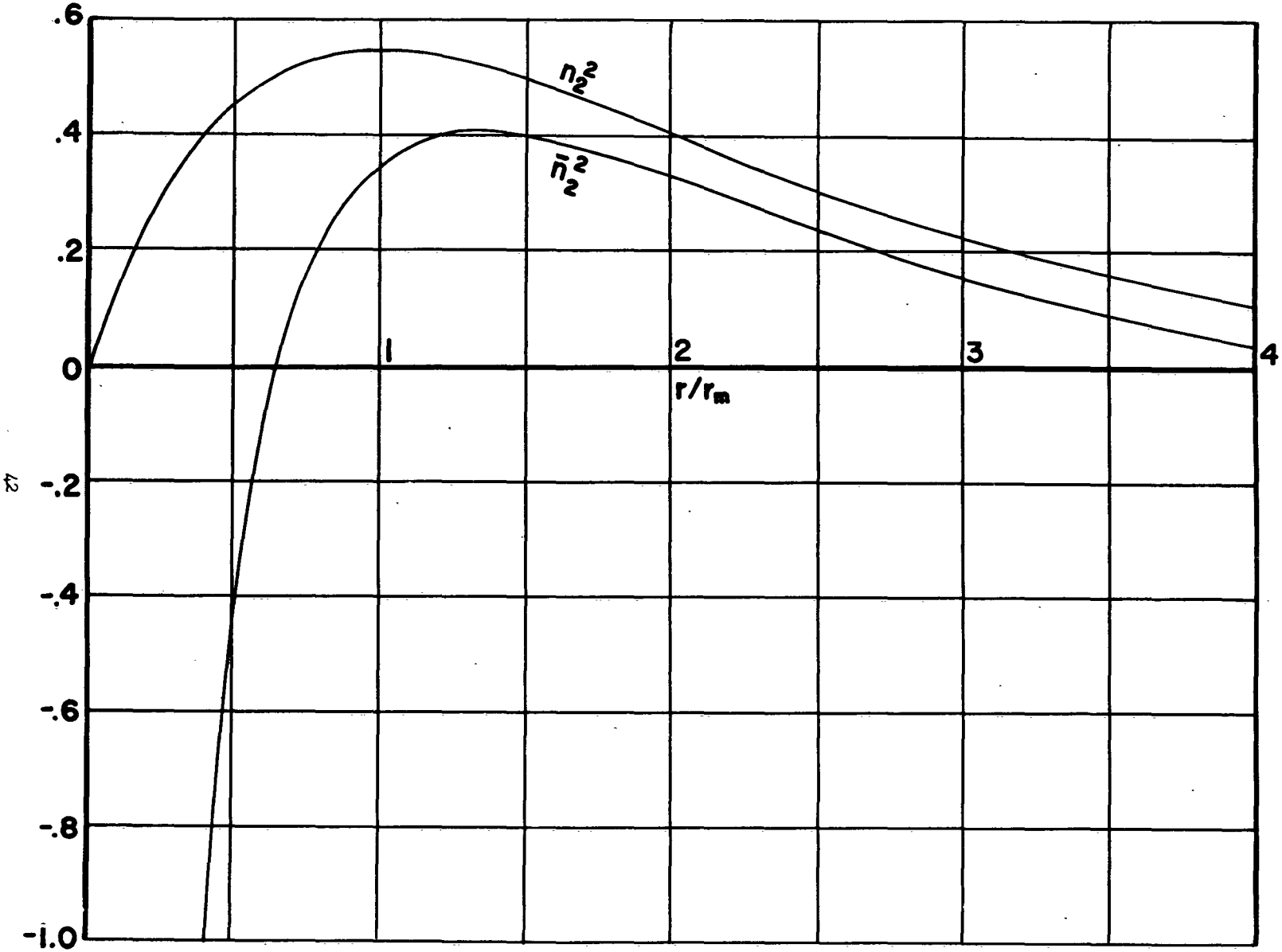

FIG. 4-1

Of course, the above example is an extreme one which is not likely to be encountered in practice. A more plausible assumption would be a case where $n_2 - 1$ was zero at $R = b$ and $R = \infty$. Nevertheless, in any model in which n_2 becomes zero at any point, $\bar{n}_2$ becomes infinite there. This is evident from

$$\bar{n}_2^2 - n_2^2 = \frac{n_2}{k_3^2} \frac{d^2(1/n_2)}{dR^2} = -\frac{n_2''}{n_2} + 2\left(\frac{n_2'}{n_2}\right)^2.$$

This is certainly infinite unless $n_2''/n_2 = 2(n_2'/n_2)^2$.

As a result of the difference in the differential equations satisfied by P^E and P^H, it is to be expected that there will be a significant difference in the behavior of the electric and magnetic modes which compose the total field when $\bar{n}_2^2$ differs greatly from n_2^2.

4.8 Discussion

In the foregoing portions of this section, the general relations for the fields and input impedance have been developed for an arbitrary spherically-stratified plasma surrounding the spherical slot antenna. It has been shown that a harmonic series representation of the fields similar to that obtained in the case of a homogeneous plasma can be developed in this case. The difference between these developments for the inhomogeneous cases lies in the form of the radial functions. This results in corresponding differences in the reflection and transmission coefficients. Consequently such characteristics as the input admittance, radiation efficiency, optimization procedures, and radiation pattern (especially at large angles to the direction of principal radiation) may be expected to be affected by the inhomogeneity of the plasma. The extent of these effects will depend on the nature and magnitude of the inhomogeneity. It was hoped that data on plasma inhomogeneity would be available for study of these effects in connection with the present work, but, unfortunately, this information was not available to us.

Some general remarks can be made regarding the effects of an inhomogeneous plasma. In Sec. 3.1 it was shown that a weak homogeneous plasma produced a change in input admittance that is directly proportional to $\nu = (n_2 - 1)$. The proof was based on a Taylor series expansion of the radial functions which involve the plasma characteristics. In the case of a weak inhomogeneous plasma, a similar result will be obtained in those cases where the corresponding radial functions (both for the electric and magnetic modes) can be expanded in a rapidly converging Taylor's series. Thus one can conclude that the result

$$\Delta Y = iK\nu + O(\nu^2)$$

obtained in Sec. 3.1 also holds for sufficiently weak inhomogeneous plasmas. The constant K, of course, will depend on the nature of the inhomogeneity, in general.

In [2] it was shown that the external efficiency of the antenna in the presence of a homogeneous plasma is the product of three factors: the ratio of power expended in the radiating modes to that delivered to all the modes, the power transmission coefficient for the radiating modes, and the transmission factor at the outer surface of the sheath (representing reflection loss at the outer boundary). In the case of an inhomogeneous plasma, the first of these factors should remain the same, while the other two could be appreciably different. An appreciable difference would be expected in cases where the overall depth of the plasma was much greater in the inhomogeneous case. For a given integrated conductivity (i.e. $\int k_2 dt$, t = thickness), the attenuation would be about the same in both cases, but the transmission factor in the inhomogeneous case would be increased appreciably from that in the homogeneous case (if the latter were small) if the plasma extended out to about a body radius.

5. VOLTAGE DISTRIBUTION ALONG THE SLOT

5.1 Introduction

In all of the analysis of the center-fed slot antenna, it has been assumed that the voltage distribution along the slot is known. For the case of a slot which is sufficiently short compared with the wavelength, the voltage distribution cannot depart appreciably from a triangular shape, either in the presence or absence of the plasma. In the numerical computation program discussed in Sec. 3, a triangular distribution was assumed.

The assumption of a triangular distribution should be a good one for sufficiently low frequencies. At higher frequencies, however, it is to be expected that the voltage distribution will depart considerably from a triangular shape. Furthermore, the distribution may change when the plasma sheath forms. Consequently, a method for determining the voltage distribution or for calculating the input admittance without requiring the assumption of a known voltage distribution would be desirable. In this Section, the efforts toward this end will be described. These efforts were not entirely successful, but a procedure which appears to hold promise is outlined.

5.2 Formulation of the Problem

The exterior admittance of a center fed spherical slot antenna was developed in [2], with the result

$$Y^e = \sum_{n=1}^{\infty} \sum_{m=0}^{n} -j \left[\frac{V_m}{V(0)}\right]^2 \frac{2\pi}{\epsilon_m \eta_1} \frac{1}{n(n+1)} \left\{ \frac{Z_n^{E1}(k_1 a)}{Z_n^{E1\prime}(k_1 a)} \left[\bar{P}_n^{m\prime}(0) I_E\right]^2 - \frac{Z_n^{H1\prime}(k_1 a)}{Z_n^{H1}(k_1 a)} \left[m \bar{P}_n^m(0) I_H\right]^2 \right\} \qquad (5.1)$$

Interchanging the order of the summations, this may be written in the form

$$Y^e = \sum_{m=0}^{\infty} \left[\frac{V_m}{V(0)}\right]^2 Y_m^e \tag{5.2}$$

where

$$Y_m^e = \sum_{n=m}^{\infty} -i\, \frac{2\pi}{\epsilon_m \eta_1 n(n+1)} \left\{ \frac{Z_n^{E1}(k_1 a)}{Z_n^{E1'}(k_1 a)} \left[\bar{P}_n^{m'}(0) I_E\right]^2 - \frac{Z_n^{H1'}(k_1 a)}{Z_n^{H1}(k_1 a)} \left[m \bar{P}_n^m(0) I_H\right]^2 \right\}. \tag{5.3}$$

In [3], a procedure was given for calculating the quantites $Z_n^{E1}(k_1 a)/Z_n^{E1'}(k_1 a)$ and $Z_n^{H1'}(k_1 a)/Z_n^{H1}(k_1 a)$ for values of n up to about 30. Consequently we may assume that approximate values of Y_m^e are available, at least for the smaller values of n.

From the expression for the azimuthal component of the magnetic field, it is readily seen that this may be written in the form

$$H_\varphi^e = \sum_{m=0}^{\infty} H_{\varphi m}^e \cos m\varphi,$$

where $H_{\varphi m}$ is independent of φ. Then it follows without difficulty from (4.21) that

$$\begin{aligned} Y^e &= \frac{1}{[V(0)]^2} \int_{-\pi}^{\pi} \int_{0}^{\pi} E_\theta^e(a,\theta,\varphi)\, H_\varphi^e(a,\theta,\varphi)\, a^2 \sin\theta\, d\theta\, d\varphi \\ &= \sum_{m=0}^{\infty} \frac{1}{[V(0)]^2} \int_{-\pi}^{\pi} \int_{0}^{\pi} E_\theta^e(a,\theta,\varphi)\, H_{\varphi m}^e(a,\theta,\varphi)\, a^2 \sin\theta \cos m\varphi\, d\theta\, d\varphi. \end{aligned} \tag{5.4}$$

Introducing the value of $E_\theta(a,\theta,\varphi)$ from (4.15), it follows on performing the φ-integration that

$$Y_m^e = \frac{2\pi a}{\epsilon_m V_m} \cdot \frac{a}{2s} \int_{\frac{\pi}{2}-\frac{s}{a}}^{\frac{\pi}{2}+\frac{s}{a}} H_{\varphi m}^e \sin\theta\, d\theta. \tag{5.5}$$

In the foregoing, V_m is the m^{th} coefficient in the Fourier expansion of the slot voltage

$$V(\varphi) = \sum_{m=0}^{\infty} V_m \cos m\varphi. \tag{5.6}$$

Up to now only the exterior admittance of the slot has been considered.

Presumably if a sufficiently simple configuration is assumed in the interior of the sphere, it would be easy to obtain the interior field and interior admittance of the slot in much the same manner as was used for the exterior. In this case, the total admittance of the slot would be

$$Y = \sum_{m=0}^{\infty} \left[\frac{V_m}{V(0)}\right]^2 Y_m \tag{5.7}$$

where

$$Y_m = Y_m^e + Y_m^i = \frac{2\pi a}{\epsilon_m V_m} \cdot \frac{a}{2s} \int_{\frac{\pi}{2}-\frac{s}{a}}^{\frac{\pi}{2}+\frac{s}{a}} (H_{\varphi m}^e - H_{\varphi m}^i) \sin\theta \, d\theta. \tag{5.8}$$

Now the m^{th} Fourier coefficient of the surface current density $K(\varphi)$ at the boundary* between the exterior field and interior field is given by the discontinuity in the m^{th} mode of the magnetic field strength

$$K_m(\theta) = H_{\varphi m}^e - H_{\varphi m}^i$$

Substituting the above into (5.8)

$$Y_m = \frac{2\pi a}{\epsilon_m V_m} \cdot \frac{a}{2s} \int_{\frac{\pi}{2}-\frac{s}{a}}^{\frac{\pi}{2}+\frac{s}{a}} K_m(\theta) \sin\theta \, d\theta, \tag{5.9}$$

or

$$Y_m = \frac{2\pi a}{\epsilon_m V_m} K_m, \tag{5.10}$$

where

$$K_m = \frac{a}{2s} \int_{\frac{\pi}{2}-\frac{s}{a}}^{\frac{\pi}{2}+\frac{s}{a}} K_m(\theta) \sin\theta \, d\theta. \tag{5.11}$$

Since the slot is assumed to be narrow ($s<<a$), the above integral is approximately equal to the m^{th} Fourier coefficient, $K_m(\theta)\big|_{\theta=\pi/2}$, of the current density at the equator.

---

* The boundary is considered to extend entirely around the equator of the sphere even though the slot extends only part of the way around it. The positive direction of surface current flow (and also of slot voltage) is taken to be the minus θ direction.

(5.10) relates the voltage across the slot

$$V(\varphi) = \sum V_m \cos m\varphi,$$

to the surface current density at the equator of the sphere

$$K(\varphi) = \sum K_m \cos m\varphi, \tag{5.12}$$

through the known quantities Y_m. Consequently (5.10), (5.12), and (5.6) should be sufficient to determine the input admittance completely without making any assumptions regarding the voltage distribution, since it should be possible to determine the latter through these equations.

5.3 Derivation of an Integral Equation for the Current Density

An integral equation for $K(\varphi)$ will be obtained in this section through use of (5.10), (5.12) and (5.6). If the m^{th} mode radiation impedance, Z_m, is defined to be the reciprocal of the m^{th} mode radiation admittance, (5.10) can be written as

$$V_m = \frac{2\pi a}{\epsilon_m} Z_m K_m. \tag{5.13}$$

Since K_m is the m^{th} coefficient in the Fourier expansion (5.12) of $K(\varphi)$, one has

$$K_m = \frac{\epsilon_m}{2\pi} \int_{-\pi}^{\pi} K(\varphi') \cos m\varphi' d\varphi'. \tag{5.14}$$

Substituting (5.14) into (5.13) and multiplying both sides by $\cos m\varphi$, there follows

$$V_m \cos m\varphi = Z_m a \cos m\varphi \int_{-\pi}^{\pi} K(m\varphi') \cos m\varphi' d\varphi'. \tag{5.15}$$

By summing (5.15) from $m = 0$ to ∞, and interchanging the order of summation and integration, (5.15) becomes

$$V(\varphi) = \int_{-\pi}^{\pi} \left[\sum_{m=0}^{\infty} Z_m \cos m\varphi \cos m\varphi'\right] K(\varphi') a d\varphi'. \tag{5.16}$$

This equation holds for all values of φ in the range $-\pi \le \varphi \le \pi$. The integral on the right hand side of the equation may be split into two parts, one representing integration from $-\varphi_1$ to $+\varphi_1$ along the slot, while the rest represents integration along the conducting surface of the sphere. Over the face of the slot the current density must be zero everywhere except at the center where it is fed. Here we set

$$K(\varphi') = I_0 \frac{1}{a} \delta(\varphi'),$$

where $\delta(\varphi')$ is the Dirac delta function and I_0 is the impressed current. Then

$$\int_{-\varphi_1}^{\varphi_1} \left[\sum_{m=0}^{\infty} Z_m \cos m\varphi \cos m\varphi'\right] K(\varphi')\, a\, d\varphi' = I_0 \sum_{m=0}^{\infty} Z_m \cos m\varphi$$

(5.16) then can be written as

$$V(\varphi) = I_0 \sum_{m=0}^{\infty} Z_m \cos m\varphi + 2\int_{\varphi_1}^{\pi} \left[\sum_{m=0}^{\infty} Z_m \cos m\varphi \cos m\varphi'\right] K(\varphi')\, a\, d\varphi', \tag{5.17}$$

where use has been made of the fact that the integrand in (5.16) must be an even function of φ', from symmetry.

If the summation in (5.17) is written as

$$G(\varphi,\varphi') \equiv \sum_{m=0}^{\infty} Z_m \cos m\varphi \cos m\varphi' \tag{5.18}$$

then (5.17) becomes

$$V(\varphi) = I_0\, G(\varphi,0) + 2a \int_{\varphi_1}^{\pi} G(\varphi,\varphi')\, K(\varphi')\, d\varphi'. \tag{5.19}$$

When φ lies in the range $\varphi_1 < |\varphi| < \pi$, $V(\varphi)$ is zero since the conducting strip in back of the slot (see Fig. 5-1) is assumed to be a perfect conductor. Consequently (5.19) becomes

$$0 = G(\varphi,0) + \int_{\varphi_1}^{\pi} G(\varphi,\varphi') \frac{2aK(\varphi')}{I_0} d\varphi' \tag{5.20}$$

if $\varphi_1 < |\varphi| < \pi$, while if $\varphi = 0$

$$Z_{in} = \frac{V(0)}{I(0)} = G(0,0) + \int_{\varphi_1}^{\pi} G(0,\varphi') \frac{2aK(\varphi')}{I_0} d\varphi'. \tag{5.21}$$

Equations (5.20) and (5.21) together with (5.18) complete the mathematical formulation of the problem. (5.20) is a Fredholm integral equation of the first kind with a symmetric kernel, $G(\varphi,\varphi')$. The unknown is the quantity $2aK(\varphi)/I_0$, which is $2a$ times the current density per unit impressed input current. If (5.20) can be solved, the input impedance, Z_{in}, will be given by (5.21). The kernel, $G(\varphi,\varphi')$, [as can be seen by substituting $\frac{1}{a}\delta(\varphi'-\varphi'')+\frac{1}{a}\delta(\varphi'+\varphi'')$ for $K(\varphi')$ in (5.16)] is numerically equal to half of the voltage at φ due to two unit source currents, symmetrically placed at $+\varphi'$ and $-\varphi'$. It is necessary to use symmetrically placed sources in (5.16) since $K(\varphi)$ was taken to be an even function of φ when it was expanded in a cosine series. If this assumption had not been made an integral equation would have been obtained with a kernel $\sum Z_m \cos m(\varphi-\varphi')$. This kernel is a Green's function, and $G(\varphi,\varphi')$ is the even part of this Green's function.

5.4 Solution of the Integral Equation for Some Special Cases

One standard method for the numerical solution of integral equations is to approximate the integral by means of a summation, and then to solve the resulting set of linear algebraic equations. Physically this corresponds, in the case treated here, to replacing the conducting strip shown in Fig. 5-1 by a number of connecting wires as shown in Fig. 5-2. The conducting surface has been replaced by $2N$ shorting wires located at $\varphi = \pm\varphi_1$, $\varphi = \pm\varphi_2$, . . . $\varphi = \pm\varphi_N \approx \pm\pi$. The current density in the region $\varphi_1 \le \varphi \le \pi$ can now be written as

$$K(\varphi) = \sum_{j=1}^{N} \frac{I_j}{a}\,\delta(\varphi-\varphi_j), \tag{5.22}$$

where I_j is the current in the wire at $\varphi = \varphi_j$.

5.4.1 Formal Solution

Substituting (5.22) into (5.20) and (5.21), and using the notation

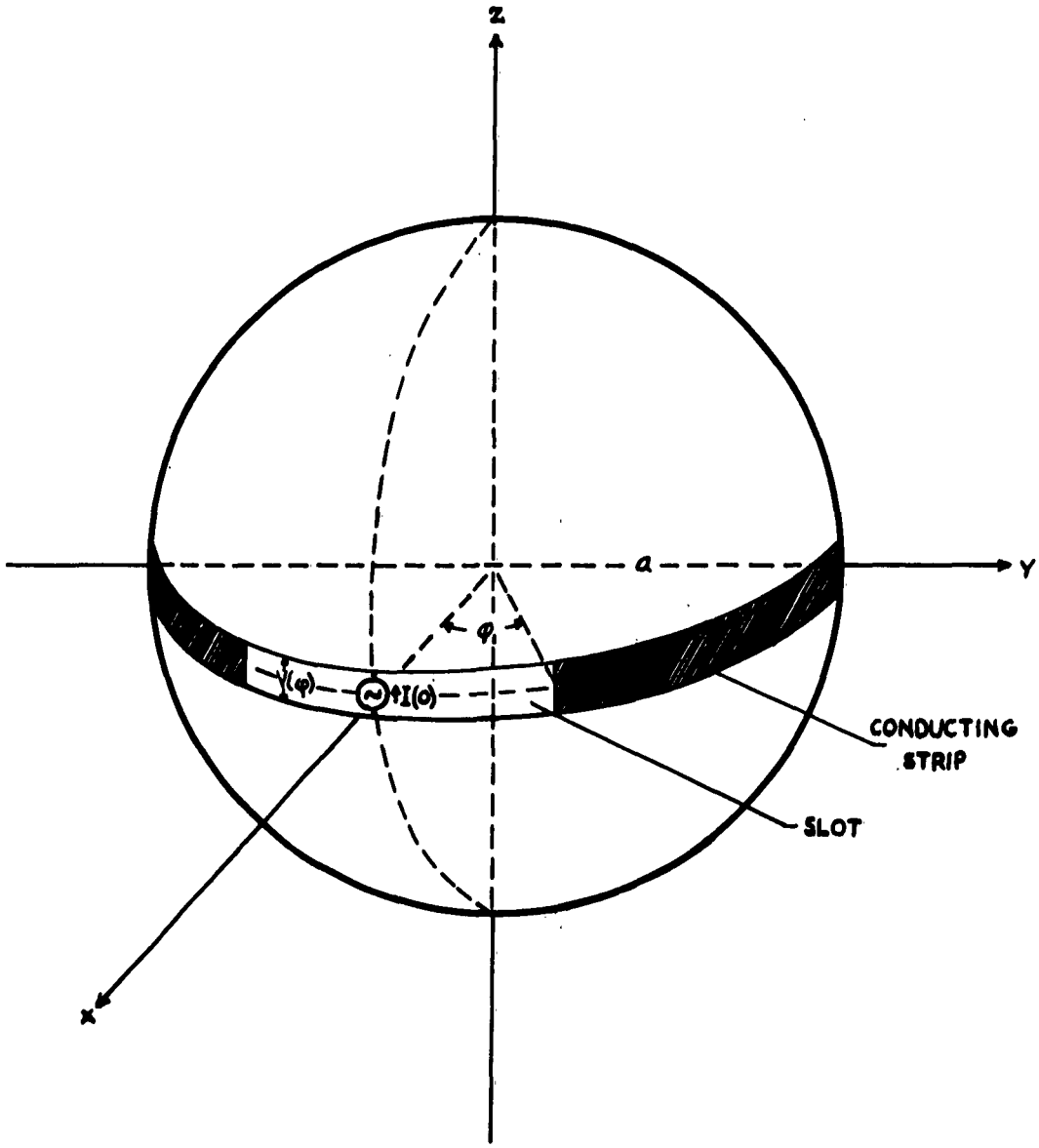
z
a
Y
φ_1
$\dot{V}(\varphi)$
$\dot{I}(\varphi)$
CONDUCTING STRIP
SLOT
x

FIG. 5-1

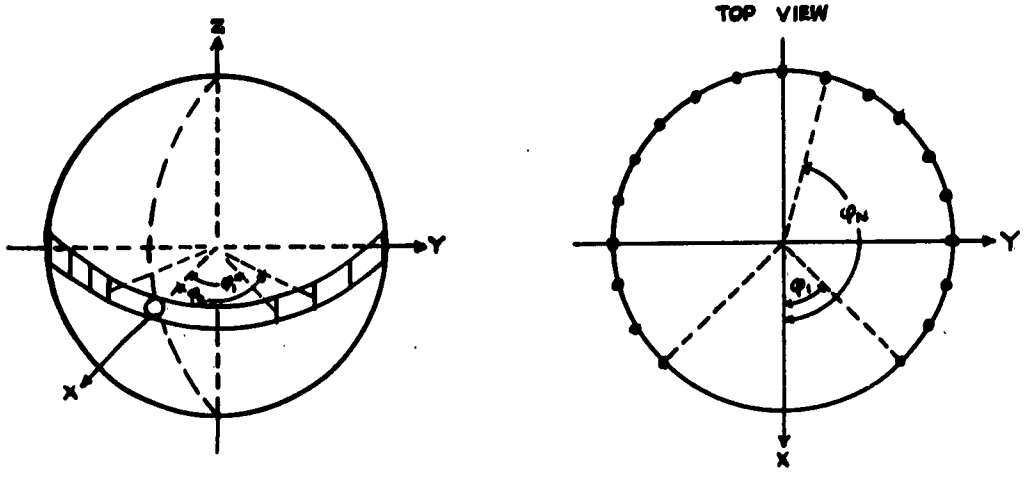

FIG. 5-2

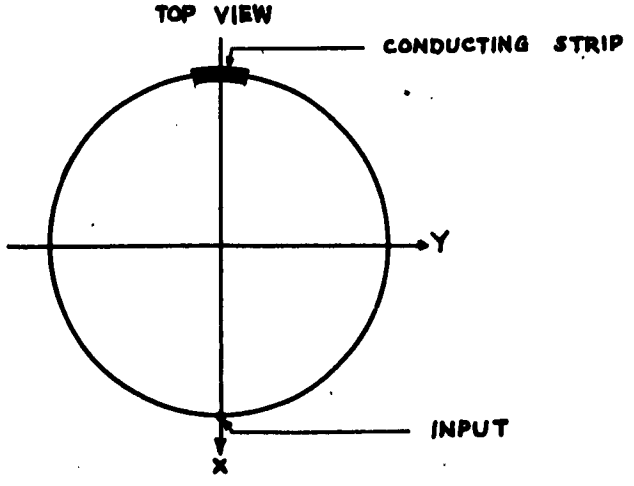

FIG. 5-3

$$G(\varphi_i, \varphi_j) \equiv G_{ij} \tag{5.23}$$

with $\varphi_0 \equiv 0$ one obtains for $i = 1, 2, \ldots N$

$$0 = G_{i0} + \sum_{j=1}^{N} G_{ij} \frac{2I_j}{I_0}, \tag{5.24}$$

$$Z_{in} = G_{00} + \sum_{j=1}^{N} G_{0j} \frac{2I_j}{I_i}, \tag{5.25}$$

or in matrix form

$$\begin{bmatrix} G_{00} & G_{01} & \cdots & G_{0N} \\ G_{10} & G_{11} & \cdots & G_{1N} \\ \cdot & \cdot & \cdots & \cdot \\ \cdot & \cdot & \cdots & \cdot \\ \cdot & \cdot & \cdots & \cdot \\ G_{N0} & G_{N1} & \cdots & G_{NN} \end{bmatrix} \begin{bmatrix} 1 \\ 2I_1/I_0 \\ \cdot \\ \cdot \\ \cdot \\ 2I_N/I_0 \end{bmatrix} = \begin{bmatrix} Z_{in} \\ 0 \\ \cdot \\ \cdot \\ \cdot \\ 0 \end{bmatrix} \tag{5.26}$$

Solving for Z_{in} by multiplying by the inverse of the matrix of the equations $[G_{ij}]$ there results

$$Z_{in} = \frac{\begin{bmatrix} G_{00} & G_{01} & \cdots & G_{0N} \\ \cdot & \cdot & \cdots & \cdot \\ \cdot & \cdot & \cdots & \cdot \\ \cdot & \cdot & \cdots & \cdot \\ G_{N0} & G_{N1} & \cdots & G_{NN} \end{bmatrix}}{\begin{bmatrix} G_{11} & G_{12} & \cdots & G_{1N} \\ \cdot & \cdot & \cdots & \cdot \\ \cdot & \cdot & \cdots & \cdot \\ \cdot & \cdot & \cdots & \cdot \\ G_{N1} & G_{N2} & \cdots & G_{NN} \end{bmatrix}} \tag{5.27}$$

where

$$G_{ij} = \sum_{m=0}^{\infty} Z_m \cos m\varphi_i \cos m\varphi_j . \tag{5.28}$$

Equations (5.27) and (5.28) provide a formal solution for the input impedance for the physical situation depicted in Fig. 5-2. This solution is correct, however, only if the matrix $[G_{ij}]$ in (5.26) has an inverse, i.e. if the numerator of (5.27) does not vanish.

Let us consider the case where the element G_{ij} defined in (5.28) is approximated using $M+1$ modes:

$$G_{ij} \approx \sum_{m=0}^{M} Z_m \cos m\varphi_i \cos m\varphi_j . \tag{5.29}$$

Then the matrix $[G_{ij}]$ can be written as a matrix product

$$\begin{bmatrix} G_{00} & \cdots & G_{0N} \\ G_{10} & \cdots & G_{1N} \\ \cdot & \cdots & \cdot \\ \cdot & \cdots & \cdot \\ \cdot & \cdots & \cdot \\ G_{N0} & \cdots & G_{NN} \end{bmatrix} = \begin{bmatrix} 1 & \cos\varphi_0 & \cdots & \cos M\varphi_0 \\ 1 & \cos\varphi_1 & \cdots & \cos M\varphi_1 \\ \cdot & \cdot & \cdots & \cdot \\ \cdot & \cdot & \cdots & \cdot \\ \cdot & \cdot & \cdots & \cdot \\ 1 & \cos\varphi_N & \cdots & \cos M\varphi_N \end{bmatrix} \begin{bmatrix} Z_0 & 0 & \cdots & 0 \\ 0 & Z_1 & \cdots & 0 \\ \cdot & \cdot & \cdots & \cdot \\ \cdot & \cdot & \cdots & \cdot \\ \cdot & \cdot & \cdots & \cdot \\ 0 & 0 & \cdots & Z_M \end{bmatrix} \begin{bmatrix} 1 & 1 & & 1 \\ \cos\varphi_0 & \cos\varphi_1 & \cdots & \cos\varphi_N \\ \cdot & \cdot & \cdots & \cdot \\ \cdot & \cdot & \cdots & \cdot \\ \cdot & \cdot & \cdots & \cdot \\ \cos M\varphi_0 & \cdot & \cdots & \cos M\varphi_N \end{bmatrix} \tag{5.30}$$

as can be verified by taking the indicated product. Now the first matrix is of order $N+1$ by $M+1$. If N is greater than M, then the determinant of the product vanishes. [See W. L. Ferrar, "Algebra" Oxford University Press, 1957, Theorem 15].

5.4.2 Impedance of a Slot Extending Completely Around the Sphere

One special case to which the formal solution (5.27) may readily be applied is that of a slot extending all of the way around the circumference of the sphere. The conducting strip in back of the slot is reduced to a narrow strip located at $\varphi_1 = \pi$, as shown in Fig. 5-3. In this case the strip evidently is equivalent to a single wire at $\varphi = \pi$, or to a single pair of symmetrically placed wires at $\varphi = \pm\pi$. Taking $\varphi_1 \equiv \varphi_N \simeq \pi$ (5.27) becomes

$$\begin{aligned} Z_{in} &= \frac{\begin{vmatrix} G_{00} & G_{01} \\ G_{10} & G_{11} \end{vmatrix}}{|G_{11}|} = \frac{\begin{vmatrix} \Sigma Z_m & \Sigma Z_m(-1)^m \\ \Sigma Z_m(-1)^m & \Sigma Z_m(-1)^{2m} \end{vmatrix}}{\Sigma Z_m(-1)^{2m}} \\ &= \frac{2\sum_m \sum_n Z_m Z_n [1-(-1)^{m+n}]}{\sum_m Z_m} \\ &= 4\frac{Z_0Z_1 + Z_0Z_3 + Z_0Z_5 + \cdots + Z_1Z_2 + Z_1Z_4 + \cdots + Z_2Z_3 + \cdots}{Z_0 + Z_1 + Z_2 + \cdots} \end{aligned} \tag{5.31}$$

5.4.3 Impedance for Two Pairs of Wires

Some additional light is shed on the general problem of the slot backed by a conducting strip if the input impedance of a slot backed by two pairs of symmetrically placed shorting wires, one pair located at $\varphi \approx \pi$ and the second pair at $\varphi = \varphi_1$, is compared with the case already calculated above in Sec. 5.2,

where the slot was backed by a single pair at $\varphi \approx \pi$ only. These two solutions for the input impedance should approach each other as φ_1 approaches π. That this is true only if some resistance is included in the shorting wires will now be shown.

If each shorting wire is replaced by a resistance R, then $V(\varphi_j)$ is equal to $-RI_j$, and equations (5.24 and (5.25) become

$$-R\frac{I_i}{I_0} = G_{i0} + \sum_{j=1}^{N} G_{ij}\,\frac{2I_j}{I_0}$$

$$Z_{in} = G_{00} + \sum_{j=1}^{N} G_{0j}\,\frac{2I_j}{I_0} \tag{5.32}$$

The solution is

$$Z_{in} = \frac{\begin{vmatrix} G_{00} & G_{01} & G_{02} & \cdots \\ G_{10} & (G_{11}+\frac{R}{2}) & G_{12} & \cdots \\ \cdot & \cdot & \cdot & \cdots \\ G_{N0} & \cdot & \cdot & (G_{NN}+\frac{R}{2}) \end{vmatrix}}{\begin{vmatrix} (G_{11}+\frac{R}{2}) & G_{12} & \cdots & G_{1N} \\ G_{21} & (G_{22}+\frac{R}{2}) & \cdots & G_{2N} \\ \cdot & \cdot & \cdots & \cdot \\ \cdot & \cdot & \cdots & (G_{NN}+\frac{R}{2}) \end{vmatrix}} \tag{5.33}$$

In the case of shorting wires at $\varphi = \varphi_1$ and $\varphi_2 \equiv \varphi_N = \pi$, this becomes

$$Z_{in} = \frac{\begin{vmatrix} G_{00} & G_{01} & G_{02} \\ G_{10} & (G_{11}+\frac{R}{2}) & G_{12} \\ G_{20} & G_{21} & (G_{22}+\frac{R}{2}) \end{vmatrix}}{\begin{vmatrix} (G_{11}+\frac{R}{2}) & G_{12} \\ G_{21} & (G_{22}+\frac{R}{2}) \end{vmatrix}} \tag{5.34}$$

Expanding as a polynomial in $R/2$

$$Z_{in} = \frac{\begin{vmatrix} G_{00} & G_{01} & G_{02} \\ G_{10} & G_{11} & G_{21} \\ G_{20} & G_{21} & G_{22} \end{vmatrix} + \frac{R}{2}\left\{ \begin{vmatrix} G_{00} & G_{01} \\ G_{10} & G_{11} \end{vmatrix} + \begin{vmatrix} G_{00} & G_{02} \\ G_{20} & G_{22} \end{vmatrix} \right\} + \frac{R^2}{4} G_{00}}{\begin{vmatrix} G_{11} & G_{12} \\ G_{21} & G_{22} \end{vmatrix} + \frac{R}{2}\left\{ G_{11} + G_{22} \right\} + \frac{R^2}{4}} \tag{5.35}$$

As $\varphi_1 \to \varphi_2$ the first terms in the numerator and denominator approach zero, since each determinant contains equal rows. If R is small, but not zero, the last term may be neglected. R cancels out of the ratio of the middle two terms leaving an expression identical to the first of equations (5.31). The limit of the indeterminate form represented by the ratio of the two leading terms of the series, however, can be shown <u>not</u> to approach (5.31)

This suggests that the resistance of the conducting strip plays a vital part in the determination of the input impedance, and that the approximation used in obtaining (5.27), namely that the resistance of the conducting strip is zero, must be made with care.

5.5 Attempted Solution of the Integral Equation

One method for obtaining a solution for the input impedance Z_{in} in (5.21) in the general case (where the conducting surface is not approximated by wires) is to approximate the kernel in (5.20) and (5.21) by a degenerate one,

$$G(\varphi, \varphi') \simeq \sum_{m=0}^{M-1} Z_m \cos m\varphi \cos m\varphi',$$

where the summation now extends over a finite number, M, of the modes instead of to infinity. This is the natural method to use since only a finite number of modes can be calculated in any case. When this is done the integral equations reduce to a set of linear algebraic equations.

If the order of summation and integration is reversed in (5.20) and the resulting equation is multiplied by $\cos n\varphi$ and integrated from φ_1 to π, one obtains

$$0 = \sum_{m=0}^{M-1} Z_{nm} T_{nm} + \sum_{m=0}^{M-1} T_{nm} Z_m X_m . \qquad (5.36)$$

Using the same procedure, (5.21) reduces to

$$Z_{in} = \sum_{m=0}^{M-1} Z_m + \sum_{m=0}^{M-1} Z_m x_m . \tag{5.37}$$

where the quantities x_m and T_{nm} are defined by

$$x_m \equiv \int_{\varphi_1}^{\pi} \cos m\varphi' \frac{2aK(\varphi')}{I_0} d\varphi' ;$$

$$T_{nm} \equiv \int_{\varphi_1}^{\pi} \cos m\varphi' \cos n\varphi' d\varphi' .$$

Inspection of (5.36) shows that a solution is given by $x_m = -1$ so that

$$Z_{in} = \Sigma Z_m - \Sigma Z_m = 0. \tag{5.38}$$

This result obviously is incorrect. The reason why an erroneous result is obtained by the above approach will be made clear in the next section where the problem will be formulated in terms of infinite matrices.

5.6 Matrix Formulation

The problem may be summarized by the five equations

$$V(\varphi) = \sum_{m=0}^{\infty} V_m U_m(\varphi) \tag{5.39}$$

$$K(\varphi) = \sum_{m=0}^{\infty} K_m(\varphi) U_m(\varphi) \tag{5.40}$$

$$V_m = (1+\delta_{0m}) Z_m a K_m \tag{5.41}$$

$$V(\varphi) = 0, \qquad \varphi_1 < |\varphi| < \pi \tag{5.42}$$

$$K(\varphi) = \frac{I_0}{a} \delta(\varphi), \qquad |\varphi| < \varphi_1 \tag{5.43}$$

where the orthonormal functions $U_n(\varphi) \equiv 1/\sqrt{(1+\delta_{0m})\pi}$ are used for mathematical convenience.

(5.41) can be written in matrix form as

$$\begin{vmatrix} V_0 \\ V_1 \\ \cdot \\ \cdot \\ \cdot \end{vmatrix} = a \begin{vmatrix} 2Z_0 & \cdot & \cdot & \cdot & \cdot \\ 0 & Z_1 & \cdot & \cdot & \cdot \\ 0 & 0 & Z_2 & \cdot & \cdot \\ \cdot & \cdot & \cdot & \cdot & \cdot \\ \cdot & \cdot & \cdot & \cdot & \cdot \end{vmatrix} \begin{vmatrix} K_0 \\ K_1 \\ \cdot \\ \cdot \\ \cdot \end{vmatrix} \tag{5.44}$$

or

$$V = aZ'K.$$

To express (5.42) and (5.43) in matrix notation, use is made of the idempotent matrix A which has the following property: A is an infinite symmetric matrix which, when it premultiplies the column matrix of the coefficients of the Fourier expansion of a given function, produces a new set of coefficients which correspond to a new function identical with the old in the region $|\varphi| < \varphi_1$, but equal to zero if $\varphi_1 < |\varphi| < \pi$. In other words, multiplication by the matrix annihilates the portion of the function which lies on the back of the slot.

The derivation of the elements of A is as follows:

Let

$$f_A(\varphi) \equiv f(\varphi), \qquad |\varphi| < \varphi_1,$$
$$\equiv 0, \qquad \varphi_1 < |\varphi| < \pi.$$

Let the Fourier expansions of $f_A(\varphi)$ and $f(\varphi)$ be

$$f_A(\varphi) = \sum_{m=0}^{\infty} f_{Am} U_m(\varphi),$$

$$f(\varphi) = \sum_{m=0}^{\infty} f_m U_m(\varphi).$$

Then

$$f_{Am} = \int_{-\varphi_1}^{+\varphi_1} f(\varphi) U_m(\varphi)\, d\varphi = \int_{-\varphi_1}^{+\varphi_1} \sum_n f_n U_n(\varphi) U_m(\varphi)\, d\varphi,$$

$$f_{Am} = \sum_n f_n \int_{-\varphi_1}^{\varphi_1} U_n(\varphi) U_m(\varphi)\, d\varphi,$$

or in matrix notation

$$f_A = Af, \tag{5.45}$$

where

$$A_{nm} = \int_{-\varphi_1}^{+\varphi_1} U_n(\varphi) U_m(\varphi)\, d\varphi$$
$$= \int_{-\varphi_1}^{\varphi_1} \frac{1}{\sqrt{(1+\delta_{0m})(1+\delta_{0n})}} \cdot \frac{1}{\pi} \cos m\varphi \cos n\varphi\, d\varphi.$$

Integrating,

$$A_{oo} = \int_{-\varphi_1}^{\varphi_1} \frac{1}{2\pi}\, d\varphi = \varphi_1/\pi, \tag{5.46a}$$

$$A_{on} = \int_{-\varphi_1}^{\varphi_1} \frac{1}{\pi\sqrt{2}} \cos n\varphi\, d\varphi = \frac{\sqrt{2}}{\pi}\frac{\sin n\varphi_1}{n}, \tag{5.46b}$$

$$A_{nm} = \int_{-\varphi_1}^{\varphi_1} \frac{1}{\pi} \cos m\varphi \cos n\varphi\, d\varphi = \frac{1}{\pi}\left[\frac{\sin(m+n)\varphi_1}{m+n} + \frac{\sin(m-n)\varphi_1}{m-n}\right] \tag{5.46c}$$

$$A_{nn} = \int_{-\varphi_1}^{\varphi_1} \frac{1}{\pi} \cos^2 n\varphi\, d\varphi = \frac{1}{\pi}\left[\frac{\sin 2n\varphi_1}{2n} + \varphi_1\right] \tag{5.46d}$$

If the function $f_B(\varphi)$ is defined by

$$f_B(\varphi) \equiv f(\varphi), \qquad \varphi_1 < |\varphi| < \pi,$$
$$\equiv 0, \qquad |\varphi| < \varphi_1,$$

then it follows from

$$f_B(\varphi) = f(\varphi) - f_A(\varphi),$$

that

$$f_{Bm} = f_m - f_{Am},$$

so that

$$f_B = (I - A)f \equiv Bf,$$

where I is the identity matrix and B is an idempotent matrix that annihilates that part of a given function that lies on the slot.

To write (5.43) in matrix form one also needs the Fourier expansion of

$$\delta(\varphi) = \sum_{m=0}^{\infty} \delta_m U_m(\varphi)$$

Then

$$\delta_m = \int_{-\pi}^{\pi} \delta(\varphi) U_m(\varphi) = U_m(0)$$

Thus

$$\delta_m = \frac{1}{\sqrt{(1+\delta_{om})\pi}}. \tag{5.48}$$

In matrix notation, then, (5.27), (5.28), and (5.29) become

$$\left.\begin{aligned} V &= aZ'K \\ BV &= O \\ AK &= \frac{I_o}{a}\delta \end{aligned}\right\} \tag{5.49}$$

where a and I_o are scalars, V and K are column matrices whose components are the coefficients in the expansions (5.39) and (5.40), δ is a column matrix with components given in (5.48), Z' is the infinite diagonal matrix displayed in (5.44), the matrix A has components given by (5.46), and the matrix B equals the identity matrix minus A.

Equations (5.49) complete the matrix formulation of the problem.

The unknown matrix V can be eliminated from (5.49) by substituting into the second equation, giving

$$\left.\begin{aligned} BZ'K &= O \\ AK &= \frac{I_o}{a}\delta \end{aligned}\right\} \tag{5.50}$$

If in (5.50) we let $K = K_B + I_o\delta/a$ we get

$$\left.\begin{aligned} BZ'K_B &= -\frac{I_o}{a}BZ'\delta \\ AK_B &= O. \end{aligned}\right\} \tag{5.51}$$

The matrices in (5.50) are infinite, so it is not strictly correct to speak of their rank or of matrix inversion. Roughly speaking, however, it is evident that the matrices A and B are in a sense singular matrices, for in (5.50) there are twice as many equations as unknowns, at least if all of the matrices involved are truncated after M modes, say.

It is now interesting to write the integral equations (5.20) and (5.21) in terms of infinite matrices: They become

$$0 = \frac{I_0}{a} B Z' \delta + B Z' K_B \tag{5.52}$$

$$Z_{in} = \pi \tilde{\delta} Z' \delta + \frac{\pi a}{I_0} \delta Z' K_B \tag{5.53}$$

Here

$$K_{Bm} = \int_{\varphi_1}^{\pi} U_m(\varphi') K(\varphi') d\varphi' \tag{5.54}$$

corresponds to the quantities x_m obtained in (5.36), where the notation used is slightly different. (5.51) can be written as

$$B Z' \left[K_B + \frac{I_0}{a} \delta \right] = 0. \tag{5.55}$$

This leads to the solution

$$K_B = -\frac{I_0}{a} \delta \tag{5.56}$$

which corresponds to the solution $x_m = -1$ obtained earlier. When the infinite matrix BZ' is truncated by using only M modes, as is done when solving the integral equation using a degenerate kernel, the truncated matrix is non-singular and (5.56) is the only solution to (5.55). It happens, however, that the truncated matrix is very nearly singular, i.e. its determinant approaches zero quite rapidly as the number of modes used is increased. This has been verified numerically using determinants of order 2, 3, and 4.

The nature of the difficulty encountered in the solution of (5.20) attempted in Sec. 5 is now clear. In approximating the infinite matrix BZ' by a finite one involving M modes, the singularity of the matrix has been destroyed and all of the non-trivial solutions to the homogeneous set of equations (5.55) have been lost. There is one more point that should be observed: the solution (5.56) is not consistent with (5.54), since δ is a matrix that corresponds to a function that vanishes in the region $\varphi_1 < |\varphi| < \pi$, while (5.54) requires that the coefficients K_{Bm} correspond to a function that vanishes in the region $|\varphi| < \varphi_1$. The above discussion makes it clear that the solution we seek is a

non-trivial solution to the homogeneous equations (5.55) that also satisfies requirement (5.54). But this solution is precisely the solution to the pair of equations (5.51).

The procedure that should be used to solve the problem is now clear. The required solution satisfies (5.51). If (5.51), which contains infinite matrices, is approximated using M modes, it reduces to a set of $2M$ equations in M unknowns. It is not expected that these equations will be exactly consistent. They should be approximately so, however, and a numerical solution should be possible. One method that suggests itself for solving (5.51) both numerically and theoretically is to use the method of least squares. The equations are first weighted by multiplying by suitable diagonal matrices W_B and W_A:

$$\begin{bmatrix} W_B B Z' \\ \cdots\cdots \\ W_A A \end{bmatrix} \begin{bmatrix} K_B \end{bmatrix} = -\frac{I_a}{a} \begin{bmatrix} W_B B Z' \delta \\ \cdots\cdots \\ 0 \end{bmatrix} \tag{5.57}$$

By premultiplying by the transpose of the magrix of the equations (5.57), there results

$$\left[Z' B W_B^2 B Z' + A W_A^2 A \right] K_B = -\frac{I_a}{a} Z' B W_B^2 B Z' \delta. \tag{5.58}$$

(5.58) above are the least squares equations for (5.51). The matrix of the equations in (5.58) is easily shown to be non-singular, [see W. L. Ferrar, loc. cit., Theorem 14], so that (5.58) may be solved using Cramer's rule. One problem that must be investigated is the proper selection of the weighting matrices W_A and W_B. That some kind of weighting is necessary is obvious on physical grounds, since the first equation in (5.51) is a relationship between voltages, while the second has the dimensions of current. Also, the results obtained in Sec. 5.4.3 suggest that it must be necessary to replace (5.50) by something like

$$\left.\begin{aligned} BZ'K &= \frac{\rho}{\pi-\varphi_1} BK \\ AK &= \frac{I_0}{a}\delta \end{aligned}\right\} \qquad (5.59)$$

where ρ is the resistivity of the conducting strip per square, and $\rho/\pi-\varphi_1$ is the total resistance of the strip, which must remain small as $\varphi_1 \to \pi$.

5.7 Summary

A formal solution for the impedance of a circumferential slot in a sphere which is fed at one point and short circuited at a number of other symmetrically located points (as in Fig. 5-2) has been given [equation (5.27)]. A simple formula (5.31) for one special case (Fig. 5-3) has been obtained. A method of attack is suggested for the general case of the impedance of a slot in a sphere (Fig. 5-1). This has not been carried through as yet.

6. THE EFFECTS OF PLASMA RADIATION ON RECEIVER NOISE

6.1 Introduction

One of the problems included in the investigations conducted under the subcontract is the analysis of the effects of a re-entry plasma upon receiving antennas aboard a hypersonic vehicle, with particular emphasis upon noise generating processes occurring in the plasma. This problem will be dealt with in this Section.

In the radiation of electromagnetic waves from a radio transmitter within a re-entry vehicle, it has been shown in previous reports that the plasma sheath produces two principal effects. These are (1) an attenuation of the transmitted wave, and (2) a lowering of the input impedance. The second effect in most cases would lead to an additional loss above that in (1) due to dissipation in the impedance matching device that would be required between the transmitter and the antenna, or to increased reflection losses if no attempt were made to restore an impedance match in the presence of the plasma sheath.

From the previous analyses, it is possible to calculate the field strength produced at a receiving point (on the ground, say) by a known voltage impressed across the antenna terminals in the vehicle. Since the input impedance of the antenna has been determined, the received field strength also can be expressed in terms of the power delivered to the transmitting antenna terminals. By the reciprocity theorem, therefore, the voltage received across the antenna terminals in the vehicle from a ground transmitter can be determined.

Although the reciprocity theorem allows the previous treatments of the transmission problem to be extended to the reception problem, this applies only to the (desired) signal. Reciprocity is strictly a two-terminal relationship, however, so that it does not consider the signal from any other source which may be

active in the received signal band. In particular, noise generated by some other source, including noise generated by the plasma, is not taken into account in such a treatment.

In determining whether a radio circuit is capable of providing reliable communication of intelligence, a criterion is adopted for a minimum signal-to-noise ratio. The noise, in many cases, is that generated in the receiver by thermal and other fluctuations in its circuits and components. The magnitude of this internal noise is dependent on the temperature of the noise-generating components, which usually is taken to be that of the surroundings. In the case of a low-noise receiver, the limiting noise is that received from external sources which radiate to the antenna. Thus a natural question arises when a high-temperature plasma surrounds the antenna of the vehicle: Is the effective noise temperature of the receiver equal to that of the plasma?

In this Section this question will be examined. It will be shown, in fact, that the effective noise temperature of the receiving system depends not alone on the temperature of the plasma, but also on the attenuation through the plasma at the frequency in question. As a consequence, a lower optimum frequency usually will exist for reception through such a plasma than for transmission.

6.2 Equivalent Noise Temperature

In dealing with the noise contributions from various sources, it is convenient to use the concept of equivalent noise temperature. It then becomes a relatively simple matter to determine the noise received by the antenna from the plasma.

The situation is identical to that encountered in the field of radio astronomy in the reception of emissions from radio noise sources. The derivation of the

well-known relations will be given here, both for completeness and to bring out the principles involved.

An antenna receives an amount of power from a radio source which depends on the emission characteristics of the source, the attenuation in the space between source and receiver, and the receiving characteristics of the antenna. The amount of power received usually is expressed in terms of an equivalent source temperature T. This temperature is that of a black body which would produce the same received power at the frequency of observation, f. From Planck's law of radiation, unit area of such a black body would radiate an amount of power per unit frequency band per unit solid angle equal to

$$E = \frac{2hf}{\lambda^2} \frac{1}{e^{hf/kT} - 1}, \tag{6.1}$$

where h is Planck's constant, and k is Boltzmann's constant. This radiation is randomly polarized. Since in most radio work $hf/kT \ll 1$, the above equation reduces to the Rayleigh-Jeans approximation

$$E = \frac{2kT}{\lambda^2}. \tag{6.2}$$

Thus the emitted power density E may be expressed in terms of the equivalent temperature T by means of (6.1), or the simplified form (6.2) if applicable. E is also called the brightness of the source.

The above concept of an equivalent brightness and equivalent temperature also may be applied to a coherent or modulated type of signal.

In observations of discrete sources, the source will subtend a solid angle Ω at the receiver which is smaller than the solid angle Ω_a of the antenna beam. The received power then is given by

$$P = \tfrac{1}{2} E B \Omega A = \frac{kTB}{\lambda^2} \Omega G \frac{\lambda^2}{4\pi} = kTB\Omega/\Omega_a \tag{6.3}$$

where B is the receiver bandwidth, $A = G\lambda^2/4\pi$ is the effective receiving area of the antenna, G its gain, and $\Omega_a = 4\pi/G$. The factor $\frac{1}{2}$ arises from the fact that

the antenna responds only to a fixed polarization, whereas the emitted radiation is assumed to be randomly polarized.

If the signal received from the desired source is to be detectable, it must be sufficiently large to produce an observable increase in the noise output of the receiver when the antenna is pointed at the source. Receiver internal noise frequently is expressed in terms of an equivalent noise temperature T_N. The noise output of the receiver in the absence of any incoming radiation from space then is the same as if a noise power

$$P_N = k T_N B \tag{6.4}$$

were supplied to the input.

This noise power also is frequently expressed in terms of the receiver "noise figure" F. This is the ratio of the actual receiver output when supplied with an available power P_o from a resistor (or other noise source), at a reference equivalent temperature T_o, to the output if T_N were zero (i.e., if the receiver generated no internal noise). Since noise powers are additive,

$$F = \frac{P_N + P_o}{P_o} = \frac{T_N + T_o}{T_o}.$$

From this,

$$T_N = (F-1)T_o. \tag{6.5}$$

The reference temperature T_o usually is taken to be 290° K. F frequently is expressed in decibels.

It is evident from the above discussion that the addition of noise powers is equivalent to the addition of the corresponding equivalent noise temperatures.

(6.4) may be used to define an equivalent temperature for the radiation received by the antenna. Denoting this by T_a, it follows from (6.3) that

$$T_a = T\Omega_A/\Omega_a. \tag{6.6}$$

In the above discussion, it has been assumed implicitly that there is free-

space transmission from source to receiving antenna. This means, among other things, that no attenuating regions between source and receiver are supposed to be present. The effect of attenuation will now be considered.

6.3 Effect of Attenuation on Receiver Noise Temperature

In considering the effect of radiation from the plasma on the noise at the input of the receiver, it is convenient to think of the plasma as a transducer. A transducer composed wholly of reactance elements generates no noise, since it possesses no mechanism for imparting random motions to the electrons circulating in its elements. Noise generation in a transducer thus is synonymous with dissipation. A transducer having a very large ($\to \infty$) loss would impart noise of temperature T_0 to the receiver, where T_0 is the transducer (ambient) temperature.

Consider, for example, a transmission line which connects an antenna to a receiver. Let the line loss factor be L (i.e., $P_{out}/P_{in} = L$), and the noise temperature of the receiver be T_N. The transmission line, through its dissipation, reduces the temperature T_a of the signal passed to the receiver to LT_a, and also contributes noise of equivalent temperature $(1-L)T_L$, where T_L is the line temperature. Hence the total noise input to the receiver is

$$T_N' = T_N + (1-L)T_L. \tag{6.7}$$

The signal-to-noise ratio thus is

$$(P_S/P_N) = LT_a/[T_N + (1-L)T_L], \tag{6.8}$$

whereas in the absence of line loss it would be

$$(P_S/P_N)' = T_a/T_N.$$

The reduction in signal-to-noise ratio thus is

$$L' = (P_S/P_N)/(P_S/P_N)' = L/[1 + (1-L)\,T_L/T_N] < L, \tag{6.9}$$

and thus is greater than the line loss factor itself.

Some numerical examples at this point may be helpful in assessing the order of magnitude of the above effect. Consider a line having an effective noise temperature of 4000°, and a receiver with a noise figure of 6 db ($F=4$). Then from (6.5)

$$T_N = 3T_0 = 870^\circ \text{ K}.$$

Suppose the line attenuation at the operating frequency is 10 db, i.e. $L = 0.1$. Then from (6.7) the effective receiver temperature is

$$T_N' = 870 + 0.9 \cdot 4000 = 4470^\circ \text{ K}.$$

Consequently the signal-to-noise ratio (in the absence of external noise) which existed in the absence of line attenuation is reduced by the factor L', which from (6.9) is

$$L' = 0.1/[1 + 0.9 \cdot 4000/870] = 0.0194 \rightarrow -17.1 \text{ db}$$

On the other hand, if the line attenuation is only 3 db, then

$$T_N' = 870 + 0.5 \cdot 4000 = 2870^\circ \text{ K}$$

and

$$L' = 0.5/[1 + 0.5 \cdot 4000/870] = 0.152 \rightarrow -8.2 \text{ db}.$$

In a similar way, a plasma surrounding a receiving antenna contributes noise to the receiver input. This noise depends both on the equivalent temperature of the plasma (T_0) and on its attenuation (L) at the frequency to which the antenna is tuned. Consequently, in a determination of an optimum frequency for reception through a re-entry plasma, the following factors are involved:

(a) the signal transfer characteristic, including

(b) the plasma attenuation;

(c) the equivalent temperature of external noise sources;

(d) the plasma temperature.

6.4 Optimization Procedures

In optimizing the power radiated from a vehicle through a re-entry plasma, only factors (a) and (b) above are involved. For the case of a strong uniform plasma, for example, we have shown [2] that the optimum frequency is the one for which the plasma thickness is $2\frac{1}{2}$ skin depths.

In the receiving case, the transfer characteristic for the signal and for external noise is the same. Consequently the ratio of signal to external noise is not affected by the plasma. But in the absence of external noise, the signal-to-noise ratio is decreased when an attenuating plasma is present, as shown by (6.8). Hence the decrease in signal-to-noise ratio due to an attenuating plasma is not as great when external noise is present than when no external noise exists.

The level of external noise is a composite of contributions from terrestrial and cosmic sources. Approximate values as a function of frequency for various locations and times are available [8] for use in planning or design purposes. In view of the great variability in external noise level, it is not possible to make an exact specification of optimum frequency for all situations. However, a typical procedure that can be followed will be illustrated below.

To illustrate the optimization procedure, consider the case of a strong uniform plasma of constant thickness. For this situation, the analysis of [2] may be used to determine the radiated fields, etc. The various factors listed at the end of Sec. 6.3 will be considered in turn.

(a) Signal transfer characteristic

For the case of a strong plasma sheath, the radiation characteristics (including sheath attenuation) are such that the high-frequency range is of interest. A slotted sphere antenna then has a radiation pattern equivalent to that of a loop whose plane is perpendicular to the center of the slot. The

far field then is given by [2, p. 22, eq. (27a)]

$$E_{\varphi'} = \frac{3\pi}{2}\frac{c}{\lambda}\frac{V_1}{1+i\chi}\frac{e^{ik_2 r}}{r}\sin\theta' \cdot e^{-ik_2(c-b)} \tag{6.10}$$

where

$$\chi = k_2(b-a).$$

For the usual case of a slot length small relative to the wavelength, the voltage distribution along the slot is approximately triangular, so that

$$V_1 = \frac{\ell}{\pi a} V(0).$$

The last factor in (6.10) represents the sheath attenuation. Denoting this attenuation by $L^{1/2}$,

$$L^{1/2} = \left|e^{-ik_2|c-b|}\right| \tag{6.11}$$

we have

$$|E_{\varphi'}| = \frac{3}{2}\frac{c}{a}\frac{\ell}{\lambda}\frac{V(0)}{|1+i\chi|}\frac{\sin\theta'}{r}L^{1/2}. \tag{6.12}$$

(6.12) gives the free-space field. The actual field at the receiver (which we assume ground-based) will be modified by propagation conditions. In order to simplify the treatment here, we will assume free-space conditions to exist in the ensuing discussion.

Let the receiving antenna have an effective gain (i.e., including line losses) of G_T, so that its effective aperture is

$$A = G_T\lambda^2/4\pi. \tag{6.13}$$

Furthermore, assume the antenna is matched to a 50-ohm line, so that the load impedance is 50 ohms. Then the power delivered to the load is

$$P_R = \frac{|E_{\varphi'}|^2 A}{120\pi} = \left(\frac{|E_{\varphi'}|\lambda}{4\pi}\right)^2 \frac{G_T}{30}$$

and consequently the load voltage is

$$V_2 = \frac{K}{|1+i\chi|}V(0)(G_T L)^{1/2}$$

$$K = \frac{(15)^{1/2} c\ell}{8\pi a}\frac{\sin\theta'}{r}$$

where the magnitude of K is independent of frequency. Hence

$$\frac{V_2}{V(0)} = \frac{K(G_T L)^{1/2}}{|1+\chi|}. \tag{6.14}$$

(6.14) gives the voltage ratio between the slot and the input to the ground-based receiver.

The coupling between the antennas in transmission from the slot antenna to the ground-based antenna can be represented as a mutual impedance, so that we can draw the equivalent circuit shown in Fig. 6-1 (a). The mesh equations are

$$V(0) = I_1^{(1)} Z_{11} + I_2^{(1)} Z_{21} \approx I_1^{(1)} Z_{11},$$

$$I_2^{(1)} Z_{22} + I_1^{(1)} Z_{21} = V_2 = -I_2^{(1)} Z_{R_2},$$

$$I_2^{(1)} = \frac{-Z_{21}}{Z_{22}+Z_{R_2}} I_1^{(1)} \approx -\frac{V(0)}{Z_{11}} \frac{Z_{21}}{Z_{22}+Z_{R_2}}.$$

For $Z_{R_2} = Z_{22} = 50$ ohms,

$$V_2 = -I_2^{(1)} Z_{R_2} = \tfrac{1}{2} V(0)\, Z_{21}/Z_{11},$$

so that

$$Z_{21} = 2 V_2 Z_{11}/V(0). \tag{6.15}$$

For the reverse case of transmission from the ground-based antenna to a receiver connected to the slot antenna, we can draw the equivalent circuit shown in Fig. 6-1 (b). In an analogous way we obtain

$$I_1^{(2)} = -\frac{Z_{12}}{Z_{11}+Z_{R_1}} I_2^{(2)} \approx -\frac{V_T}{Z_{22}} \frac{Z_{12}}{Z_{11}+Z_{R_1}}. \tag{6.16}$$

By the reciprocity theorem, $Z_{12} = Z_{21}$ so that from (6.15) and (6.16)

$$V_1 = -I_1^{(2)} Z_{R_1} = \frac{V_T}{Z_{22}} \frac{Z_{12} Z_{R_1}}{Z_{11}+Z_{R_1}} = \frac{V_T V_2}{V(0)} \frac{Z_{11}}{Z_{22}} \frac{Z_{R_1}}{Z_{11}+Z_{R_1}}.$$

Assuming that the receiver input is tuned optimally (by an automatic tuning device, for example) so that

$$Z_{R_1} = Z_{11}^*,$$

the above equation reduces to

$$V_1 = \frac{V_T V_2}{V(0)} \frac{Z_{11}}{Z_{22}} \frac{Z_{11}^*}{2R_1} = \frac{V_T V_2}{V(0)} \frac{1}{100 R_{11} |Y|^2} = \frac{V_T V_2}{V(0)} \frac{1}{100 g}, \tag{6.17}$$

where $g = \mathcal{R}_e(Y)$ is the input conductance of the slot. In the above we have taken $Z_{22} = 50$.

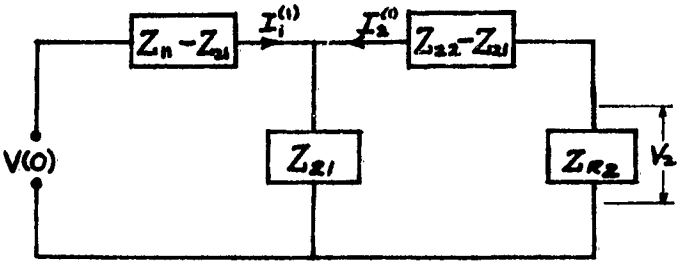
$Z_{11}-Z_{21}$
$I_1^{(1)}$
$I_2^{(1)}$
$Z_{22}-Z_{21}$
V(0)
Z_{21}
Z_{R2}
V_2

(a)

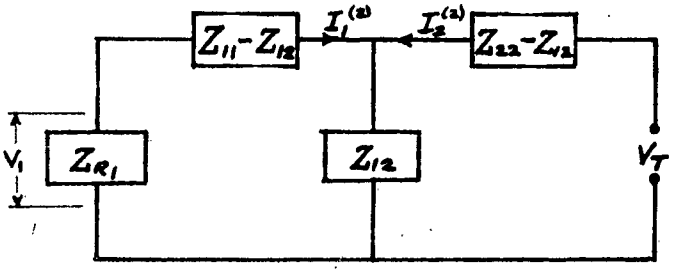
$Z_{11}-Z_{12}$
$I_1^{(2)}$
$I_2^{(2)}$
$Z_{22}-Z_{12}$
V_1
Z_{R1}
Z_{12}
V_T

(b)

FIG. 6-1

V_T may be expressed in terms of the transmitted power P_T, since

$$P_T = V_T^2/Z_{22}. \tag{6.18}$$

Since the signal power P_s' at the receiver input is $V_1^2 \mathcal{G}$, we have

$$P_s' = \left(\frac{P_T G_T}{4\mathcal{G}} \frac{K^2}{|1+\lambda\chi|^2}\right) L \equiv \mathcal{S} L, \tag{6.19}$$

where $\mathcal{S}$ may be called the signal transfer characteristic. P_s' is equivalent to a signal temperature T_s',

$$T_s' = P_s'/kB. \tag{6.20}$$

In the absence of the sheath, the signal power would be

$$P_s = \frac{P_T G_T}{4\mathcal{G}'} \frac{3\lambda^2 \sin^2\theta'}{8\pi r^2} \equiv \frac{P_T G_T}{4\mathcal{G}'} K_1^2 \lambda^2, \tag{6.21}$$

where

$$K_1^2 = \frac{3}{8\pi}\left(\frac{\sin\theta'}{r}\right)^2.$$

The frequency-dependent terms in $\mathcal{S}$ of (6.19) are G_T, $\mathcal{G}$ and χ. For a ground-based antenna of constant effective aperture, $G_T \propto \lambda^2$, while $\chi \propto \lambda^{-1/2}$. $\mathcal{G}$ may be found from calculated values of Y. Consequently we may calculate the signal transfer characteristic $\mathcal{S}$ and plot a curve of it as a function of frequency.

(b) Plasma attenuation

The plasma attenuation is given by

$$L = \left|e^{-ik_2(c-b)}\right|.$$

But for a highly conducting plasma

$$k_2 = (-i\omega\mu_0\sigma_0)^{1/2} = \left(\frac{-i\omega\mu_0\epsilon_0\omega_N^2}{\nu}\right)^{1/2} = \frac{\omega_N}{v}\left(\frac{\omega}{\nu}\right)^{1/2} e^{-i\pi/4},$$

where ω_N is the radian plasma frequency, ν the collision frequency, and v the velocity of light. Hence

$$L = e^{-2\Re(k_2)\cdot(c-b)} = e^{-\frac{\omega_N}{v}\left(\frac{\omega}{2\nu}\right)^{1/2}(c-b)} \tag{6.22}$$

L thus decreases exponentially as the square-root of frequency. From known (or estimated) values of ω_N and ν, L may be calculated and plotted against frequency.

(c) Equivalent temperature of external noise

External noise is a combination of terrestrial (natural + man-made) and cosmic noise. The noise level is a complicated function of location, time (of day and season), as well as of frequency. For planning purposes, curves published by the CCIR [8] may be used. These curves actually give the equivalent noise temperature, F_a, expressed in db relative to $T_o = 288°$ as a reference. Hence a curve of external noise temperature vs. frequency may be selected for the location and time of interest. This noise temperature, however, applies for a receiving antenna which is a short (relative to the wavelength) grounded vertical rod. Since such an antenna has a gain of 3/2 relative to an isotropic antenna, the CCIR noise temperatures should be multiplied by 2/3 (i.e., decreased by roughly 2 db).

In making use of the CCIR curves, it is necessary to assume that the external noise is uniformly distributed over all directions. This actually is not true, since, for example, natural terrestrial noise is due to thunderstorms, which are not uniformly distributed; nor are propagation characteristics, which are superimposed on the source distribution, independent of direction. In accordance with the above assumption of a uniform distribution of external noise, the solid angle Ω of the source is 4π. Hence from (6.5) and (6.6) the external noise temperature at the antenna is

$$T_E = (F_a - 1) T_o \frac{4\pi}{4\pi/G} = \frac{3}{2}(F_a - 1) \cdot 288 = 432(F_a - 1), \qquad (6.23)$$

where the gain of the antenna has been taken to be 3/2.

Since external noise experiences the same reduction in passing through the plasma sheath as does the signal, the temperature of external noise at the receiver may be obtained by multiplying (6.23) by the ratio P_3/P_3' obtained from (6.19) and (6.21):

$$T_E' = \frac{P_s}{P_s'} T_E = \frac{K^2 \mathcal{G}'}{K_1^2 \mathcal{G}} \frac{L}{|1+i\chi|^2 \lambda^2} \cdot 432(F_a - 1) \qquad (6.24)$$

Values of T_E' may be calculated from (6.24) and plotted as a function of frequency.

(d) Equivalent plasma temperature

The equivalent plasma temperature already has been discussed in Sec. 6.3. If we denote the plasma temperature by T_P, then from (6.7) the total noise temperature of the receiver (excluding external noise) is

$$T_N' = T_N + (1-L) T_P. \qquad (6.25)$$

Since L (and possibly T_N) is a function of frequency, values of T_N' may be plotted vs. frequency from (6.22) and data on T_N.

From the plotted curves of the various factors discussed in (a) - (d) above, it is a simple matter to combine these to obtain a curve of the overall signal-to-noise ratio at the receiver. This is given by

$$\frac{T_S'}{T_E' + T_N'} = \frac{P_S'}{\mathcal{R}[T_E' + T_N + (1-L)T_P]B}$$

where P_s' is given by (6.19), T_E' by (6.24), and L by (6.22). From such a curve, the optimum frequency can be determined.

In general, because of the large effect of plasma attenuation both in reducing the signal level and in raising the internal noise level, it is to be expected that the optimum frequency for reception will be lower than the optimum frequency for transmission. The extent to which one can gain in reception by lowering the frequency is determined largely by the external noise level. The latter is a strong function of geographical location and temporal factors, so that the optimum frequency for reception will vary accordingly.

7.0 CONCLUSIONS AND RECOMMENDATIONS

7.1 Conclusions

7.1.1 Calculations of Input Admittance

A study of calculations of input admittance of a spherical slot antenna made by MSVD on the IBM 704 revealed two significant phenomena and two limitations:

(a) A linear relation exists between the change in input admittance from the free-space value and the change in refractive index, as expressed in the relation

$$\Delta Y = iK(n_2 - 1)$$

for small $(n_2 - 1)$.

(b) An apparent interference phenomenon takes place for small collision frequencies around a certain value of plasma frequency.

(c) The calculations are erroneous for certain values and ranges of the parameters.

(d) The series formulation used is not practical for values of vehicle circumference greater than about one wavelength.

7.1.2 Theoretical Extensions

The following results were obtained in extension of previous developments:

(a) The relation for ΔY given above in Sec. 7.1.1 (a) is shown to exist for any vehicle size. This suggests a useful technique for preflight calibration of the antenna so that in-flight measurements may be used to determine plasma properties.

(b) The phenomenon mentioned in Sec. 7.1.1.(b) is explained as the interference produced by reflections from the outer boundary of the plasma sheath, whereby the antenna is effectively terminated by an almost pure reactance.

(c) An analysis of the input admittance which is suitable for large vehicle sizes is outlined.

7.1.3 Inhomogeneous Plasmas

A general formulation is given of the problem of an inhomogeneous spherical plasma. It is shown that the previous forms of the result are still retained, the only change being that the radial functions require alteration. In this connection, a significant new feature is that the electric and magnetic modes satisfy different differential equations.

7.1.4 Slot Voltage Distribution

The determination of the voltage distribution along the slot in the general case leads to an integral equation. A practical solution to this problem was not found, but a method of attack which may prove fruitful is presented.

7.1.5 Plasma Noise

In a discussion of the effect of noise generated in the plasma upon the reception problem, it is shown that the effective noise temperature of a receiving system aboard a re-entry vehicle depends on the attenuation of the plasma as well as on the plasma temperature. Consequently, the optimum frequency for reception usually will be significantly lower than for transmission.

7.2 Recommendations

1. In view of the inaccuracies of the double precision program used in the calculations, it is recommended that a triple precision program be employed in any future calculations.

2. The practical importance of a calibration technique based on the relation $\Delta Y = \lambda K(n_2-1)$ makes it desirable to extend the validity of this expression to geometries other than spherical.

3. In Sec. 3.3, a procedure was outlined whereby practically useful formulas can be obtained for large spheres. The details of this procedure should be worked out so that formulas suitable for numerical computation will be available.

4. In Sec. 4, formulations were derived for inhomogeneous plasmas. It is recommended that these formulations be applied to available information on plasma properties, so that the quantitative effects of plasma inhomogeneities on antenna radiation properties can be deduced.

5. The effect of the plasma on the voltage or current distribution along an antenna is still an unsolved problem. In view of its importance in upper atmospheric research, further work on this problem is justified.

6. The effect of noise generated by the plasma on reception aboard a re-entry vehicle has been shown in Sec. 6 to lead to lower optimum working frequencies in reception than in transmission. It is recommended that experiments aimed at verifying this conclusion be considered.

8.0 REFERENCES

1. General Electric Subcontracts PO 214-60175 and PO 214-60301.
2. J.W. Marini, B.Y.-C. Koo, M. Katzin, "Radiation and Impedance of Antennas Surrounded by an Ionized Sheath", ERC Report 60301-6, 25 Aug. 1958.
3. J.W. Marini, B.Y-C Koo, J.K. Buckley, "Calculation of the Effect of an Ionized Sheath on the Admittance of an Insulated Spherical Slot Antenna", ERC Report 61527-1, 21 April 1959.
4. Martin Katzin and Benjamin Y.-C. Koo, "The Effect of an Inhomogeneous Plasma on Antenna Radiation. I. An Exact Earth-Flattening Procedure in Propagation Around a Sphere", ERC Report No. 61527-2, 9 June 1959.
5. W. Franz, "Theorie der Beugung Elektromagnetischer Wellen", Springer, 1957.
6. B. Friedman, "Propagation in a Non-Homogeneous Atmosphere", Comm. Pure & App. Math., 4, 317-350, Aug. 1951.
7. L.L. Bailin and S. Silver, "Exterior Electromagnetic Boundary Value Problems for Spheres and Cones", I.R.E. Trans. PGAP, AP-4, 5-16, Jan. 1956.
8. CCIR, Documents of the IXth Plenary Assembly, vol. III, Report No. 65, pp. 223-256, Geneva 1959.